The Journal of Chemical Physics ARTICLE pubs.aip.org/aip/jcp

Kinetic theory of chiral active disks: Odd transport and torque density

Cite as: J. Chem. Phys. 165, 034501 (2026); doi: 10.1063/5.0332479
Submitted: 4 March 2026 • Accepted: 26 June 2026 •
Published Online: 15 July 2026

View Online Export Citation CrossMark

Raphaël Maire,[1,a] Alessandro Petrini,[2] Umberto Marini Bettolo Marconi,[3] and Lorenzo Caprini[2,a]

AFFILIATIONS

[1] Department of Condensed Matter, University of Barcelona, 08028 Barcelona, Spain
[2] Sapienza University of Rome, IT-00185 Rome, Italy
[3] Università di Camerino, Scuola di Scienze e Tecnologie, 62032 Camerino, Italy

[a] **Authors to whom correspondence should be addressed:** maire@ub.edu and lorenzo.caprini@uniroma1.it

ABSTRACT

Parity-odd transport is a central signature of chiral fluids, yet analytical predictions are sparse. Here, we introduce a minimal two-dimensional hard-disk gas in which chirality arises solely from a collision-induced transverse impulse. Motivated by granular spinners, collisions are dissipative and inject orbital angular momentum through a fixed tangential "kick" at contact. Starting from a Boltzmann–Enskog description, we derive nonlinear hydrodynamic equations for density, momentum, and temperature and show that chirality generates an antisymmetric homogeneous stress corresponding to a nonzero torque density. In the dilute limit, a Chapman–Enskog expansion yields analytical predictions for transport coefficients, including odd viscosity, odd thermal conductivity, and odd self-diffusivity, in good agreement with numerical simulations. This minimal kinetic model can serve as a foundation for systematic coarse-graining of chiral fluids and as a tractable benchmark for gaining insight into odd transport across a broader class of chiral systems.

Published under an exclusive license by AIP Publishing. https://doi.org/10.1063/5.0332479

15 July 2026 13:12:18

I. INTRODUCTION

Chiral active matter encompasses a broad class of systems that break parity symmetry at the level of their microscopic constituents.[1,2] Representative examples range from microswimmers—such as sperm cells and bacteria moving along circular trajectories near surfaces[3,4]—to microorganisms, including cells,[5] algae,[6] and starfish embryos,[7] which exhibit the formation of rotating clusters. Chiral particles have also been artificially engineered by designing micro- or macroscopic objects with broken rotational symmetry. Notable examples include chiral active colloids moving along circular paths[8] and granular spinners that self-rotate due to external driving mechanisms such as light,[9] internal motors,[10] vibrating plates,[11–14] or airflows.[15,16]

A wealth of distinctive phenomena characterizes these chiral systems.[17–21] In particular, a circularly moving object that breaks parity symmetry typically exhibits edge currents along confining boundaries,[22–25] circulating currents in the presence of an external confining potential,[26] as well as rotating crystallites in solid structures.[27,28] These effects originate from their non-standard diffusive properties, which couple different Cartesian components of the motion. As a consequence, Fick's law governing the density evolution involves a diffusion matrix with antisymmetric off-diagonal components. These terms are commonly referred to as odd diffusion[16,25,29–31] or odd mobilities[32,33] and have been analytically predicted starting from microscopic models of chiral active particles.[29,34,35] Related diffusive responses and mobilities have also been reported in magnetic skyrmions due to gyrotropic effects.[36–38]

More broadly, the behavior of chiral systems is often described using hydrodynamic theories for the density and momentum fields, reminiscent of generalized Navier–Stokes equations operating far from equilibrium. In contrast to conventional fluids, the viscosity tensor of a two-dimensional chiral system contains antisymmetric components, known as odd viscosity coefficients (see Ref. 39 for a review). Odd viscosity[39–42] was first introduced in hydrodynamic theory by Avron[43] and has recently been observed experimentally both in active-matter systems[44] and in electron fluids.[45] Unlike bulk and shear viscosity, odd viscosity does not dissipate energy, yet it can induce Hall-like transport[46] and lift forces.[47,48]

Although the recent literature on the hydrodynamics of chiral fluids is rapidly growing,[39,49] derivations or analytical predictions

Published under an exclusive license by AIP Publishing

of odd transport coefficients remain scarce. Recently, hydrodynamic equations for chiral active fluids were derived[50] from the Langevin dynamics of chiral particles subject to odd interactions,[51] i.e., effective transverse forces that generate a net torque.[52–55] This work showed that chiral fluids are not only characterized by odd viscosity—as assumed in most hydrodynamic treatments—but also by a chirality-induced torque density.[39,56,57] However, odd viscosity is often introduced phenomenologically, on symmetry grounds, rather than derived microscopically from the underlying many-body physics. Notable exceptions are Ref. 58, which used linear-response theory to obtain an interaction-induced odd viscosity in the dilute limit for rotating particles undergoing binary collisions, and Ref. 59, which developed a Chapman–Enskog theory of energy- and momentum-conserving chirally colliding hard disks.

Here, we present one of the first analytical studies predicting transport coefficients for chiral fluids. We derive explicit expressions for the torque density, odd viscosity, odd thermal conductivity, and odd self-diffusivity within a kinetic theory in which chirality arises solely from the collision-induced injection of orbital angular momentum. Motivated by granular systems, particle collisions are dissipative yet inject energy transversely to the line connecting the particle centers (see Fig. 1 for an illustration). This collision rule is the instantaneous analog of odd interactions, where a transverse interparticle force represents, at a coarse-grained level, the effective coupling between two rotating particles. Such forces may be mediated by hydrodynamic interactions in a surrounding fluid or arise from the rotational friction of granular spinners.

We introduce the model in Sec. II, summarize the main results in Sec. III, and present the derivations in Sec. IV. We conclude with a discussion.

II. MODEL

We consider a chiral active fluid consisting of N hard disks of diameter σ and mass m, moving in a box of size L with periodic boundary conditions. Motivated by kinetic models typical of driven granular gases, particles move ballistically until they undergo binary collisions, where chirality manifests through an injection of angular momentum. Specifically, when two particles 1 and 2 come into contact ($|\mathbf{r}_1 - \mathbf{r}_2| = \sigma$), their velocities are updated via an active, parity-breaking collision rule,

$$\boldsymbol{v}_1' = \boldsymbol{v}_1 - \frac{1+\alpha}{2}(\boldsymbol{v}_{12}\cdot\hat{\boldsymbol{\sigma}}_{12})\hat{\boldsymbol{\sigma}}_{12} - \Delta\hat{\boldsymbol{\sigma}}_{12}^{\perp}, \tag{1a}$$

$$\boldsymbol{v}_2' = \boldsymbol{v}_2 + \frac{1+\alpha}{2}(\boldsymbol{v}_{12}\cdot\hat{\boldsymbol{\sigma}}_{12})\hat{\boldsymbol{\sigma}}_{12} + \Delta\hat{\boldsymbol{\sigma}}_{12}^{\perp}, \tag{1b}$$

where $\hat{\boldsymbol{\sigma}}_{12} = (\mathbf{r}_1 - \mathbf{r}_2)/\sigma$, $\boldsymbol{v}_{12} = \boldsymbol{v}_1 - \boldsymbol{v}_2$, and $\boldsymbol{v}_1$ and $\boldsymbol{v}_1'$ are the velocities of particle 1 before and after the collision, respectively.

The term $(1+\alpha)(\boldsymbol{v}_{12}\cdot\hat{\boldsymbol{\sigma}}_{12})\hat{\boldsymbol{\sigma}}_{12}/2$ corresponds to the inelastic hard-disk normal impulse. Like a repulsive force, this term reverses the normal component of the relative velocity and reduces its magnitude. Indeed, the post-collisional velocity is related to the pre-collisional one through the following relation involving the restitution coefficient $0 \le \alpha \le 1$:

$$(\boldsymbol{v}_{12}'\cdot\hat{\boldsymbol{\sigma}}_{12}) = -\alpha(\boldsymbol{v}_{12}\cdot\hat{\boldsymbol{\sigma}}_{12}). \tag{2}$$

Consequently, $\alpha = 1$ corresponds to elastic hard-disk collisions without energy dissipation, while $\alpha < 1$ dissipates kinetic energy at each collision.

The second term, $\Delta\hat{\boldsymbol{\sigma}}_{12}^{\perp}$, is an active tangential impulse that breaks parity symmetry and is generated by a chiral mechanism. Here, $\hat{\boldsymbol{\sigma}}_{12}^{\perp} = \boldsymbol{\varepsilon}\cdot\hat{\boldsymbol{\sigma}}_{12} = (\hat{\sigma}_{12,y}, -\hat{\sigma}_{12,x})$ with $\boldsymbol{\varepsilon}$ the two-dimensional Levi–Civita symbol ($\varepsilon_{xy} = -\varepsilon_{yx} = 1$). Therefore, Δ has the dimension of a velocity and sets the magnitude of a fixed transverse "kick" at contact, with its handedness controlled by $\mathrm{sign}(\Delta)$. Equivalently, this term corresponds to a singular nonconservative contact force with an odd (transverse) component, and it breaks the conservation of *orbital* angular momentum in each collision, providing a microscopic source of chiral stresses. The equilibrium hard-disk limit corresponds to $\Delta \to 0$ and $\alpha = 1$, while $\Delta \to 0$ and $\alpha < 1$ yield a freely cooling granular gas.[60]

The collision rule can alternatively be expressed in terms of an impulsive force $\mathbf{F}_{12}$ acting on particle 1 due to particle 2,

$$\mathbf{F}_{12} = -m\left(\frac{1+\alpha}{2}(\boldsymbol{v}_{12}\cdot\hat{\boldsymbol{\sigma}}_{12})\hat{\boldsymbol{\sigma}}_{12} + \Delta\hat{\boldsymbol{\sigma}}_{12}^{\perp}\right)\delta(t - t_{12}^{\mathrm{coll}}), \tag{3}$$

where $\delta(t - t_{12}^{\mathrm{coll}})$ is the Dirac delta function at collision time t_{12}^{coll}. The force $\mathbf{F}_{12}$ can be considered an impulsive odd interaction, which typically governs the dynamics of chiral active particles. Indeed, $\mathbf{F}_{12}$ is nonconservative because it cannot be derived from a potential and has a component acting transversely to the direction connecting the particles' centers.[51,52,61] Such odd interactions are coarse-grained descriptions of transverse forces generated by rotation, either through hydrodynamic coupling between rotating objects in a fluid[7,62,63] or through rotational friction in granular spinners. Motivated by the latter, we also include dissipative collisions by taking $\alpha < 1$.

In contrast to other chiral models that include self-rotation[58,64–71] or self-propulsion,[72–77] our model has neither rotational nor orientational degrees of freedom. Instead, chirality emerges solely from the injection of orbital angular momentum during collisions (Fig. 1). This may be the simplest model for chiral systems, where collisions inject angular momentum and energy via Δ, which is dissipated through the restitution coefficient α, leading to a nonequilibrium steady state.

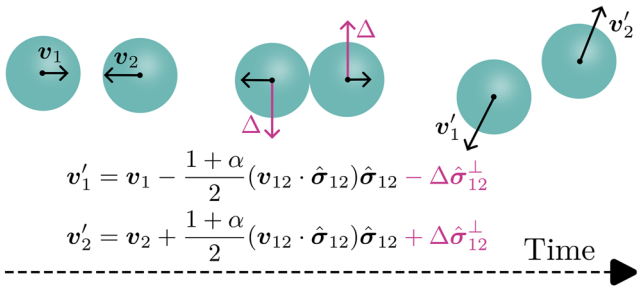

FIG. 1. Illustration of a typical collision between two chiral active particles, labeled 1 and 2, following the collision rule (II). The post-collisional velocities $\boldsymbol{v}_1'$ and $\boldsymbol{v}_2'$ are characterized by (i) a reduced *normal* magnitude due to dissipation, as in conventional granular particles ($\alpha < 1$), and (ii) an additional velocity component transverse to the line connecting the particle centers, generated by chirality.

15 July 2026 13:12:18

Published under an exclusive license by AIP Publishing

We simulate the system through event-driven molecular dynamics simulations.[78] Since the only microscopic dimensional parameters are σ, m, and Δ, velocities are measured in units of $|\Delta|$, energies such as kinetic temperature $T = \frac{m}{2N}\sum_i \boldsymbol{v}_i^2$ in units of $m\Delta^2$, and times in units of $\sigma/|\Delta|$. We thus fix the transverse velocity injection Δ and use the packing fraction $\phi = N\pi\sigma^2/4L^2 = n\pi\sigma^2/4$ and restitution coefficient α as control parameters. A strict equilibrium limit is unattainable at fixed Δ. As $\alpha \to 1$, the normal component of collisions becomes elastic and non-dissipative, while collisions continue to inject energy and angular momentum; as a consequence, the steady-state kinetic temperature grows without bound. In this limit, the chiral energy injected per collision becomes asymptotically negligible. Indeed, we will show that $T \simeq m\Delta^2/(1-\alpha^2)$ so that $m\Delta^2/T \sim 1-\alpha^2 \ll 1$ as $\alpha \to 1$. Most chiral effects are therefore expected to be most pronounced at small α, where $T \simeq m\Delta^2$, and at large ϕ, since collisions are the source of chirality.

This chirality gives rise to new macroscopic phenomena, including odd transport coefficients and a nonzero torque density. We now describe these effects and summarize our main results.

III. RESULTS OVERVIEW

The many-body dynamics resulting from the kinetic model with collision rule (II) is governed by hydrodynamic equations for the slow fields at large scales.[79] Number density $n(\mathbf{r},t)$ and momentum $mn(\mathbf{r},t)\boldsymbol{u}(\mathbf{r},t)$ are locally conserved, so their relaxation times are set by the observation scale. While the kinetic temperature $T(\mathbf{r},t)$ is not conserved for $\alpha < 1$ or $\Delta \neq 0$, it remains a slow field close to $\alpha = 1$ and $\Delta = 0$ and should therefore be included in the hydrodynamic description.[60,80]

We obtain the following hydrodynamic balance equations at coarse-grained scales:

$$\partial_t n + \boldsymbol{u}\cdot\nabla n = -n\nabla\cdot\boldsymbol{u}, \tag{4a}$$

$$\partial_t \boldsymbol{u} + \boldsymbol{u}\cdot\nabla\boldsymbol{u} = \frac{1}{mn}\nabla\cdot\left(\boldsymbol{\Pi}^{\mathrm{homo}} + \boldsymbol{\Pi}^{\mathrm{visc}}\right), \tag{4b}$$

$$\partial_t T + \boldsymbol{u}\cdot\nabla T = \frac{1}{n}(\boldsymbol{\Pi} : \nabla\boldsymbol{u} - \nabla\cdot\boldsymbol{J}) + \delta\dot{T}, \tag{4c}$$

where $\boldsymbol{\Pi} = \boldsymbol{\Pi}^{\mathrm{homo}} + \boldsymbol{\Pi}^{\mathrm{visc}}$ denotes the stress tensor, decomposed into homogeneous and viscous contributions. The quantity $\boldsymbol{J}$ represents the heat current, while $\delta\dot{T}$ denotes the rate of energy change due to collisions.

As a first main result, we discover that the homogeneous stress tensor $\boldsymbol{\Pi}^{\mathrm{homo}}$ includes not only the hydrostatic pressure p but also a torque density[81] $\tau = \boldsymbol{\varepsilon} : \boldsymbol{\Pi}^{\mathrm{homo}}/2$,

$$\boldsymbol{\Pi}^{\mathrm{homo}} = -p\boldsymbol{I} + \tau\boldsymbol{\varepsilon} = \begin{pmatrix} -p & \tau \\ -\tau & -p \end{pmatrix}. \tag{5}$$

This torque density is a direct consequence of the tangential forces during collisions acting as a source of angular momentum and will be shown to be given by

$$\tau = n\phi\chi m\sqrt{\frac{4\pi\Delta^2}{1-\alpha^2}}\Delta, \tag{6}$$

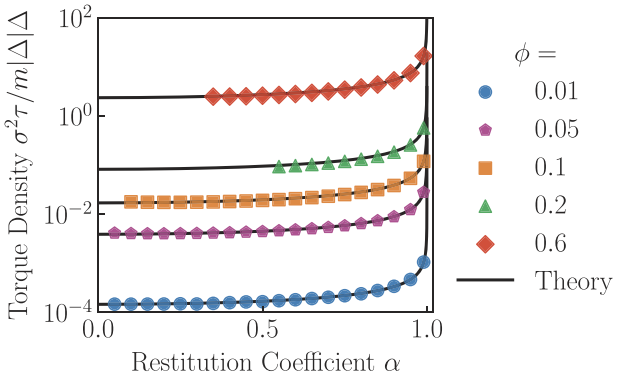

FIG. 2. Comparison between numerical measurements and theoretical predictions [Eq. (6)] for the torque density τ as a function of the restitution coefficient α. The results are obtained for $N = 10^4$ particles, with each data point averaged over at least 10^3 independent snapshots. Here, we include only data showing a homogeneous configuration. Therefore, numerical measurements at low α are not included since the system exhibits an inhomogeneous phase reminiscent of the bubble phase numerically observed in Refs. 51, 54, 83, and 84.

where χ is the pair correlation at contact, which we approximate by its equilibrium hard-disk value.[82] The term τ has the same sign as the chiral parameter Δ and diverges as $\alpha \to 1$. This divergence reflects an unbounded rate of angular-momentum injection, which arises from the diverging temperature and collision frequency in the same limit. We find excellent agreement between the measured τ in our simulations and Eq. (6) in Fig. 2, even at high densities.

Our second main result is the analytical prediction for regular and odd transport coefficients[39,40] in the dilute limit via a Chapman–Enskog expansion. Specifically, the viscous stress

$$\Pi_{ij}^{\mathrm{visc}} \equiv \eta_{ijkl}\partial_k u_l, \tag{7}$$

depends on the velocity gradient and the viscosity tensor $\boldsymbol{\eta}$, with repeated indices implicitly summed. In a two-dimensional, isotropic but parity-breaking fluid, η_{ijkl} can be decomposed into a basis of six independent isotropic tensors built from δ_{ij} and ε_{ij}. A physically motivated decomposition is[39]

$$\begin{aligned}\eta_{ijkl} = {} & \eta_s(\delta_{ik}\delta_{jl} + \delta_{il}\delta_{jk} - \delta_{ij}\delta_{kl}) + \zeta\delta_{ij}\delta_{kl} + \eta_o(\varepsilon_{ik}\delta_{jl} + \varepsilon_{jl}\delta_{ik}) \\ & - \eta_B\delta_{ij}\varepsilon_{kl} - \eta_A\varepsilon_{ij}\delta_{kl} + \eta_R\varepsilon_{ij}\varepsilon_{kl},\end{aligned} \tag{8}$$

where η_s and η_o denote the even and odd shear viscosities, respectively. Odd viscosity, in contrast to the (even) shear viscosity, is nondissipative: the odd-viscous stress is orthogonal to the velocity gradient and, therefore, does not produce viscous heating, $\Pi_{ij}^{\mathrm{odd}}\partial_i u_j = 0$. In simple shear, $u_x = \dot{\gamma}y$, it yields an anisotropic, pressure-like response rather than a frictional shear stress.[85] Within the dilute approximation considered here, all viscosity coefficients other than η_o and η_s vanish in our system, and, remarkably, we are able to report one of the first analytical expressions for η_o as an explicit function of the model parameters,

$$\eta_o = \frac{2m(1-\alpha)}{\chi\sigma(1+\alpha)P(\alpha)}\Delta, \tag{9}$$

15 July 2026 13:12:18

Published under an exclusive license by AIP Publishing

where $P(\alpha)$ is a positive polynomial defined in Appendix C 3. As expected, η_o changes sign with the chiral parameter Δ and vanishes when $\Delta \to 0$ but also as $\alpha \to 1$, showing that dissipative collisions are required to generate odd viscosity in our model. Measurements of η_o are compared with theory in Fig. 3(a) and show good agreement at low density.

The temperature expression in Eqs. (4) reflects the balance between mechanical work, heat transport, and active energy injection. The heat current is

$$\boldsymbol{J} = -\kappa \nabla T - \kappa_o(\boldsymbol{\varepsilon} \cdot \nabla) T, \tag{10}$$

where κ is the regular thermal conductivity and κ_o, its parity-odd counterpart.[58,86] Unlike odd viscosity, odd thermal conductivity is subtler because $\nabla \cdot (\kappa_o \boldsymbol{\varepsilon} \cdot \nabla T) = (\nabla \kappa_o) \cdot (\boldsymbol{\varepsilon} \cdot \nabla T)$ since $\varepsilon_{ij}\partial_i\partial_j T = 0$. Hence, κ_o does not enter the *linearized bulk* temperature dynamics about a uniform state, but it affects boundary heat currents and contributes nonlinearly when $\kappa_o(n, T)$ varies in space. Within our theory, we find the value of κ_o to be

$$\kappa_o = \frac{8(1-\alpha)}{\chi \sigma Q(\alpha)} \Delta, \tag{11}$$

with $Q(\alpha)$ a positive polynomial defined in Appendix C 4. Once again, this odd coefficient vanishes in the limit $\alpha \to 1$. Overall, the theory and simulations agree well, as seen in Fig. 3(b), with the low-density discrepancies most likely due to systematic measurement errors, as will be explained later.

Before deriving these results, we briefly comment on transport coefficients that do not enter the hydrodynamic equations [Eqs. (4)]. Since the fluid velocity is conserved and density is governed solely by the continuity equation with no diffusive flux, there is no mass-diffusion mode in the hydrodynamic equations. Nonetheless, treating a fluid particle as a tracer in the effective bath formed by the other particles leads to an effective diffusion equation for the tracer density, with current

$$\boldsymbol{J}_s = -D \nabla n_s - D_o(\boldsymbol{\varepsilon} \cdot \nabla) n_s, \tag{12}$$

where D and D_o are the regular and odd self-diffusivities,[25,29] respectively. As for the odd thermal conductivity, the effect of the odd diffusivity primarily enters through boundary conditions. We predict D_o to be given by

$$D_o = \frac{\pi \sigma}{2\phi\chi(1+\alpha)R(\alpha)} \Delta, \tag{13}$$

with $R(\alpha)$ a positive polynomial defined in Appendix C 5. This coefficient does not vanish in the limit $\alpha \to 1$ and is very well predicted by the theory, as shown in Fig. 3(c).

All other regular transport coefficients, as well as the pressure and temperature, are also well captured by our theory and are presented later in the article. We now explain how these expressions are derived.

IV. RESULTS DERIVATION

All analytical derivations and integral evaluations appearing implicitly or explicitly in this section were performed symbolically using SymPy[87] in a notebook provided in the supplementary material.

A. Boltzmann equation

Because collisions are instantaneous and strictly binary, the microscopic dynamics in Eqs. (1) admit an approximate description in terms of a Boltzmann–Enskog equation[60,88]

$$\partial_t f(\mathbf{r}_1, \boldsymbol{v}_1, t) + \boldsymbol{v}_1 \cdot \nabla f(\mathbf{r}_1, \boldsymbol{v}_1, t) = \mathcal{J}(\mathbf{r}_1, \boldsymbol{v}_1 | f, f), \tag{14}$$

where f is the single-particle distribution for observing a particle at time t with position $\mathbf{r}_1$ and velocity $\mathbf{v}_1$. The term $\mathcal{J}$ represents the collision operator, accounting for the velocity change at a given position due to a collision with another particle. This operator can be obtained by counting the number of collisions per unit of time at $(\mathbf{r}_1, \boldsymbol{v}_1)$ in phase space, i.e., by calculating $\nu(\mathbf{r}_1, \boldsymbol{v}_1, \boldsymbol{v}_2, \hat{\boldsymbol{\sigma}}_{12}) d\mathbf{r}_1 d\boldsymbol{v}_1 d\boldsymbol{v}_2 d\hat{\boldsymbol{\sigma}}_{12}$, where ν is the differential collision

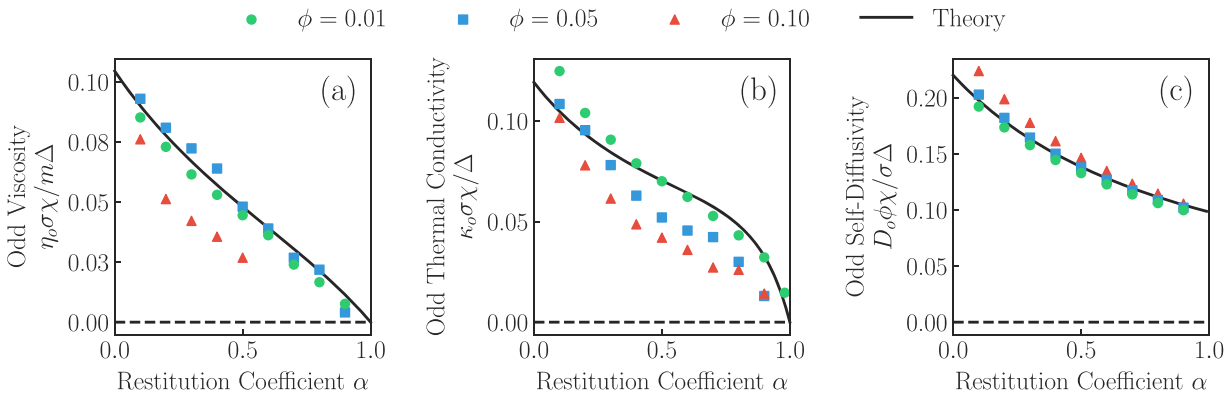

FIG. 3. Odd transport coefficients as functions of the restitution coefficient α—which also sets the strength of chirality—at three different packing fractions, $\phi = 0.01, 0.05, 0.1$. (a) Odd viscosity measured from an imposed shear flow, as detailed in Appendix A 2. The missing data points for $\phi = 0.1$ correspond to systems in which the smallest numerically accessible shear rate was still too large to yield reliable measurements. (b) Odd thermal conductivity measured using a Green–Kubo relation (see Appendix A 3). (c) Odd self-diffusivity measured using a Green–Kubo relation (see Appendix A 4). Solid lines show theoretical predictions [Eqs. (9), (11), and (13)], while dashed lines indicate the corresponding values for a nonchiral system.

15 July 2026 13:12:18

Published under an exclusive license by AIP Publishing

frequency, proportional to the relative speed and the scattering cross section, encoding the probability of a binary collision with impact direction $\hat{\boldsymbol{\sigma}}_{12} = (\mathbf{r}_1 - \mathbf{r}_2)/\sigma$. For hard-disks,[60] the collision frequency can be expressed as $\nu(\mathbf{r}_1, \boldsymbol{v}_1, \boldsymbol{v}_2, \hat{\boldsymbol{\sigma}}_{12}) = f_2(\mathbf{r}_1, \mathbf{r}_2, \boldsymbol{v}_1, \boldsymbol{v}_2)\sigma|\boldsymbol{v}_{12} \cdot \hat{\boldsymbol{\sigma}}_{12}|$, with f_2 the two-particle density distribution function calculated at the coordinate of the second particle, $\mathbf{r}_2 = \mathbf{r}_1 - \sigma\hat{\boldsymbol{\sigma}}_{12}$ and $\boldsymbol{v}_{12} = \boldsymbol{v}_1 - \boldsymbol{v}_2$. Collisions can remove particles from velocity $\boldsymbol{v}_1$ (loss term) or bring particles from some pre-collisional velocity $\boldsymbol{v}_1''$ into $\boldsymbol{v}_1$ (gain term),

$$\tilde{\mathcal{J}}(\mathbf{r}_1, \boldsymbol{v}_1) = -\int \Theta(-\boldsymbol{v}_{12} \cdot \hat{\boldsymbol{\sigma}}_{12})\nu(\mathbf{r}_1, \boldsymbol{v}_1, \boldsymbol{v}_2, \hat{\boldsymbol{\sigma}}_{12})d\boldsymbol{v}_2 d\hat{\boldsymbol{\sigma}}_{12} + \int \Theta(-\boldsymbol{v}_{12}'' \cdot \hat{\boldsymbol{\sigma}}_{12})\nu(\mathbf{r}_1, \boldsymbol{v}_1'', \boldsymbol{v}_2'', \hat{\boldsymbol{\sigma}}_{12})d\boldsymbol{v}_2'' d\hat{\boldsymbol{\sigma}}_{12}, \quad (15)$$

with Θ the Heaviside function ensuring head-on collisions and $\boldsymbol{v}''$ the pre-collisional velocities that produce $\boldsymbol{v}$ after a collision. Inverting the collision rule [Eqs. (1)] yields

$$\boldsymbol{v}_1'' = \boldsymbol{v}_1 - \frac{1+\alpha^{-1}}{2}(\boldsymbol{v}_{12} \cdot \hat{\boldsymbol{\sigma}}_{12})\hat{\boldsymbol{\sigma}}_{12} + \Delta\hat{\boldsymbol{\sigma}}_{12}^{\perp}, \quad (16a)$$

$$\boldsymbol{v}_2'' = \boldsymbol{v}_2 + \frac{1+\alpha^{-1}}{2}(\boldsymbol{v}_{12} \cdot \hat{\boldsymbol{\sigma}}_{12})\hat{\boldsymbol{\sigma}}_{12} - \Delta\hat{\boldsymbol{\sigma}}_{12}^{\perp}. \quad (16b)$$

Since ν depends on the two-particle distribution density function, the evolution equation for f is not closed. To proceed, we adopt the molecular chaos closure, which neglects velocity–velocity and velocity–position correlations at collision,[89]

$$f_2(\mathbf{r}_1, \mathbf{r}_2, \boldsymbol{v}_1, \boldsymbol{v}_2) = \chi(\mathbf{r}_1, \mathbf{r}_2)f(\mathbf{r}_1, \boldsymbol{v}_1)f(\mathbf{r}_2, \boldsymbol{v}_2), \quad (17)$$

where $\chi(\mathbf{r}_1, \mathbf{r}_2) \equiv \chi[n((\mathbf{r}_1 + \mathbf{r}_2)/2)]$ corresponds to the pair correlation function $\chi[n]$ at contact evaluated at the local midpoint density,[88] taking into account short-range spatial correlations arising from the finite size of the particles.

Putting everything together and changing variables $\boldsymbol{v}'' \to \boldsymbol{v}$ in the second term of Eq. (15), we obtain the collision operator of the Boltzmann–Enskog equation[60]

$$\mathcal{J}(\mathbf{r}_1, \boldsymbol{v}_1|f, f) = \sigma \int \Theta(-\boldsymbol{v}_{12} \cdot \hat{\boldsymbol{\sigma}}_{12})|\boldsymbol{v}_{12} \cdot \hat{\boldsymbol{\sigma}}_{12}|\chi(\mathbf{r}_1, \mathbf{r}_2) \times \left[\frac{f(\mathbf{r}_1, \boldsymbol{v}_1'')f(\mathbf{r}_2, \boldsymbol{v}_2'')}{\alpha^2} - f(\mathbf{r}_1, \boldsymbol{v}_1)f(\mathbf{r}_2, \boldsymbol{v}_2)\right] \times d\boldsymbol{v}_2 d\hat{\boldsymbol{\sigma}}_{12}. \quad (18)$$

Here, the prefactor $1/\alpha^2$ in the gain term comes from two contributions: (i) the Jacobian of the linear change of variables $(\boldsymbol{v}_1'', \boldsymbol{v}_2'') \mapsto (\boldsymbol{v}_1, \boldsymbol{v}_2)$, which yields $d\boldsymbol{v}_2'' = (1/\alpha)d\boldsymbol{v}_2$, and (ii) the transformation of the collision rate, which involves the normal relative velocity $|\boldsymbol{v}_{12}'' \cdot \hat{\boldsymbol{\sigma}}_{12}| = (1/\alpha)|\boldsymbol{v}_{12} \cdot \hat{\boldsymbol{\sigma}}_{12}|$ for the inelastic rule. Neither the Jacobian nor the normal-rate factor is affected by the chiral parameter Δ, since it induces only an *additive* and *transverse* change of the velocities. The shorthand $\mathcal{J}(\mathbf{r}_1, \boldsymbol{v}_1|f, f)$ highlights the bilinear dependence of the collision operator on the single-particle distributions of the two colliding particles, $f(\mathbf{r}_1, \boldsymbol{v}_1)$ and $f(\mathbf{r}_2, \boldsymbol{v}_2)$. We keep this bilinear structure explicit, since later we will also consider mixed terms of the form $\mathcal{J}(\mathbf{r}_1, \boldsymbol{v}_1|f, g)$, where g is a function distinct from f.

Equation (14) is a nonlinear and nonlocal integro-differential equation and is therefore difficult to analyze. We first familiarize ourselves with it by considering the spatially homogeneous state.

B. Homogeneous probability distribution

Our objective is to derive hydrodynamic equations from the microscopic collision rule [Eq. (1)]. Before coarse-graining, we note that non-gradient observables, such as the homogeneous stress, are already accessible in the spatially uniform steady state, where time and space derivatives vanish. Consequently, Eq. (14) reduces to

$$\mathcal{J}(\boldsymbol{v}|f, f) = 0, \quad (19)$$

which determines the steady-state single-particle distribution $f(\mathbf{r}, \boldsymbol{v}, t) \equiv f(\boldsymbol{v}, t)$. In the equilibrium limit ($\alpha \to 1$ and $\Delta \to 0$), detailed balance yields a Maxwellian shape, whereas here dissipation and parity-breaking may drive a nontrivial steady state.

We first assess whether non-Gaussianities are quantitatively important by simulating the microscopic dynamics defined by the collision rule (II). Figure 4(a) shows the steady-state velocity distribution in the dilute regime. At weak normal dissipation ($\alpha = 0.99$), the velocity distribution $f(\boldsymbol{v})$ is effectively Gaussian. As shown in Appendix B, this behavior stems from the divergence of the temperature as $\alpha \to 1$, which makes the nonequilibrium chiral contribution asymptotically negligible. In this limit, $m\Delta^2 \ll T$, and the system approaches an equilibrium-like regime. As dissipation $(1 - \alpha)$ increases, chiral effects become more prominent relative to the temperature T ($m\Delta^2 \simeq T$), leading to small but systematic overpopulated tails. In the dilute limit $\phi \to 0$, these tails can be treated perturbatively by expanding f in Sonine polynomials, which form an orthogonal basis with respect to the Gaussian weight.[60] The derivation of this expansion beyond the Gaussian case is reported in Appendix B. The results of this expansion are presented in Fig. 4(b) via the 2D excess kurtosis $\kappa_{\text{ex}} \equiv \langle \boldsymbol{v}^4 \rangle / \langle \boldsymbol{v}^2 \rangle^2 - 2$, which quantifies deviations from Gaussianity since $\kappa_{\text{ex}} = 0$ for a Gaussian distribution. The Sonine prediction is in good agreement with simulations at low packing fractions ϕ, independently of the restitution coefficient α. However, its accuracy deteriorates at higher densities, where velocity correlations at collisions invalidate the molecular-chaos assumption[89] [see Eq. (17)]. A Sonine expansion cannot capture the resulting non-Gaussian features of the velocity distribution, which are notoriously difficult to treat analytically.[90,91] Since Sonine corrections are quantitatively small in the regime of interest, we neglect them in the following. They can be straightforwardly reintroduced, at the expense of more cumbersome expressions.

We note that chiral hard-particle models with internal spin can exhibit pronounced non-Gaussian statistics,[58] which can limit quantitative accuracy. Since chirality in our model arises without internal rotation, non-Gaussian corrections remain small.

C. Homogeneous temperature and stress

The homogeneous temperature is defined through the velocity fluctuations as

$$T = \frac{m}{2n}\int \boldsymbol{v}^2 f(\boldsymbol{v})d\boldsymbol{v}. \quad (20)$$

15 July 2026 13:12:18

Published under an exclusive license by AIP Publishing

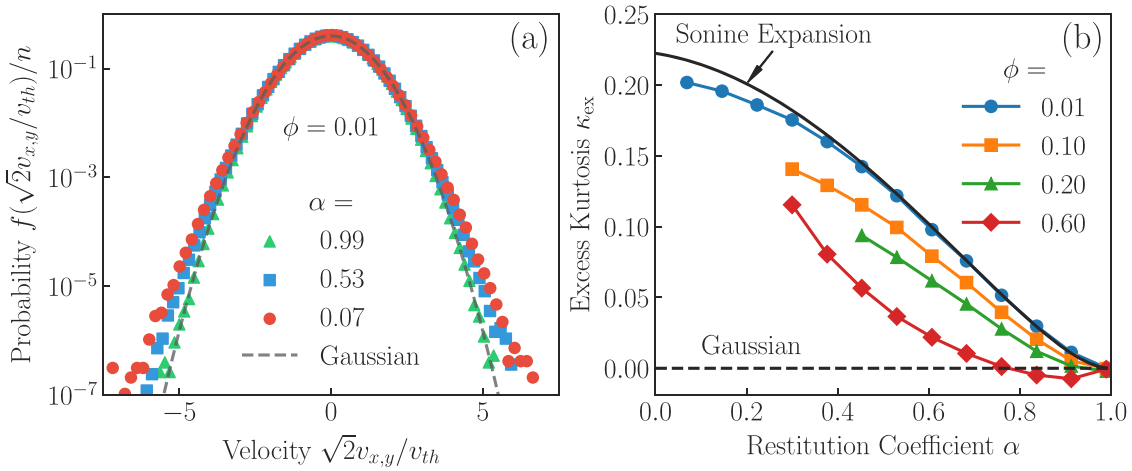

FIG. 4. Comparison of the steady-state velocity probability distribution $f(v)$ between simulations ($N = 5000$) and theory. (a) Distribution of the normalized velocity in a dilute system ($\phi = 0.01$) for several values of the restitution coefficient α. We use $v_{th} = \sqrt{2T/m}$ so that the distributions have unit variance. (b) Excess kurtosis κ_{ex} as a function of α at different packing fractions. Solid and dashed lines show theoretical predictions: $\kappa_{ex} = 0$ corresponds to a Gaussian distribution, while a Sonine expansion predicts $\kappa_{ex} \neq 0$ in the dilute limit where molecular chaos holds. The data at low α are omitted for some values of ϕ when the system develops inhomogeneous configurations, reminiscent of those observed in Refs. 51, 54, 83, and 84.

Since we consider a Gaussian approximation $f(\boldsymbol{v})$, motivated by Fig. 4(a),

$$f(\boldsymbol{v}) = \frac{mn}{2\pi T} e^{-\frac{m\boldsymbol{v}^2}{2T}}, \tag{21}$$

the temperature field can be identified with the variance of the distribution. Multiplying Eq. (14) by $m\boldsymbol{v}^2$ and integrating over $\boldsymbol{v}$ yields an evolution equation for the temperature[92,93] (see Appendix C 1)

$$\partial_t T(t) = \frac{\omega(\phi, T)}{2} \langle \delta E \rangle_{\text{coll}} \equiv \delta \dot{T}, \tag{22}$$

where $\delta E \equiv m(\boldsymbol{v}_1'^2 + \boldsymbol{v}_2'^2 - \boldsymbol{v}_1^2 - \boldsymbol{v}_2^2)/2$ is the energy change at collision and ω is the collision frequency per particle.[89] As a consequence, the term $\omega\langle \delta E \rangle_{\text{coll}}$ coincides with the average rate of energy change due to collisions and can be expressed as

$$\omega \langle \delta E \rangle_{\text{coll}} = \sigma \chi n^{-1} \int \Theta(-\boldsymbol{v}_{12} \cdot \hat{\boldsymbol{\sigma}}_{12}) |\boldsymbol{v}_{12} \cdot \hat{\boldsymbol{\sigma}}_{12}| \times \delta E f(\boldsymbol{v}_2) f(\boldsymbol{v}_1) d\hat{\boldsymbol{\sigma}}_{12} d\boldsymbol{v}_1 d\boldsymbol{v}_2. \tag{23}$$

Imposing stationarity in Eq. (22) yields a theoretical prediction for the temperature (see Appendix C 2),

$$T_{\text{Gauss}} = \frac{m\Delta^2}{1-\alpha^2}, \tag{24}$$

which follows from the condition $0 = \langle \delta E \rangle_{\text{coll}} = m\Delta^2 - (1-\alpha^2)T$. This steady-state temperature is independent of packing fraction because higher density increases the collision rate but not the *average* energy exchanged per collision in the steady state, leaving the balance unchanged.[93] In practice, the breakdown of molecular chaos invalidates this argument.

Even in the limit $\alpha \to 1$ at finite density, we find $T_{\text{sim}}/T_{\text{theory}} \neq 1$, indicating that nonequilibrium correlations beyond molecular chaos persist even though the velocity distribution f is nearly Gaussian. At moderate packing fractions ϕ, small deviations from a Gaussian distribution manifest as a weak density dependence of T, demonstrating the breakdown of molecular chaos. Nevertheless, the temperature is overall well captured by Eq. (24), as shown in Figs. 5(a) and 5(b), and the agreement can be further improved by including a Sonine correction (see Appendix B).

The homogeneous stress can be computed without invoking the Boltzmann equation by using the standard expression for the virial stress,[79]

$$\boldsymbol{\Pi}^{\text{virial}} = -\frac{\sum_{\alpha=1}^{N} m\boldsymbol{c}_\alpha \otimes \boldsymbol{c}_\alpha - \sigma \sum_{\alpha<\beta}^{N} \hat{\boldsymbol{\sigma}}_{\alpha\beta} \otimes \mathbf{F}_{\alpha\beta}}{L^2}, \tag{25}$$

where $\boldsymbol{c}_\alpha = \boldsymbol{v}_\alpha - \langle \boldsymbol{v} \rangle$ is the deviation of the velocity of particle α from the local average velocity and $\mathbf{F}_{\alpha\beta}$ is the singular force given in Eq. (3). In the homogeneous state, the average virial stress coincides with the homogeneous stress tensor $\langle \boldsymbol{\Pi}^{\text{virial}} \rangle = \boldsymbol{\Pi}^{\text{homo}}$. The interaction term arises from collisions and can be obtained from a time average over a window $\mathcal{T}$, which reduces to a collisional average,[94,95]

$$\begin{aligned} \langle \hat{\boldsymbol{\sigma}}_{\alpha\beta} \otimes \mathbf{F}_{\alpha\beta} \rangle &= \mathcal{T}^{-1} \int_0^{\mathcal{T}} \hat{\boldsymbol{\sigma}}_{\alpha\beta}(t) \otimes \mathbf{F}_{\alpha\beta}(t) dt \\ &= \mathcal{T}^{-1} \sum_{\text{all}} \sum_{\alpha\beta} \sum_{\text{coll.}} \hat{\boldsymbol{\sigma}}_{\alpha\beta}(t_{\alpha\beta}^{\text{coll}}) \otimes \mathbf{I}_{\alpha\beta}(t_{\alpha\beta}^{\text{coll}}) \\ &= \frac{\omega(\phi, T)}{2} \langle \hat{\boldsymbol{\sigma}}_{\alpha\beta} \otimes \mathbf{I}_{\alpha\beta} \rangle_{\text{coll}}. \end{aligned} \tag{26}$$

15 July 2026 13:12:18

Published under an exclusive license by AIP Publishing

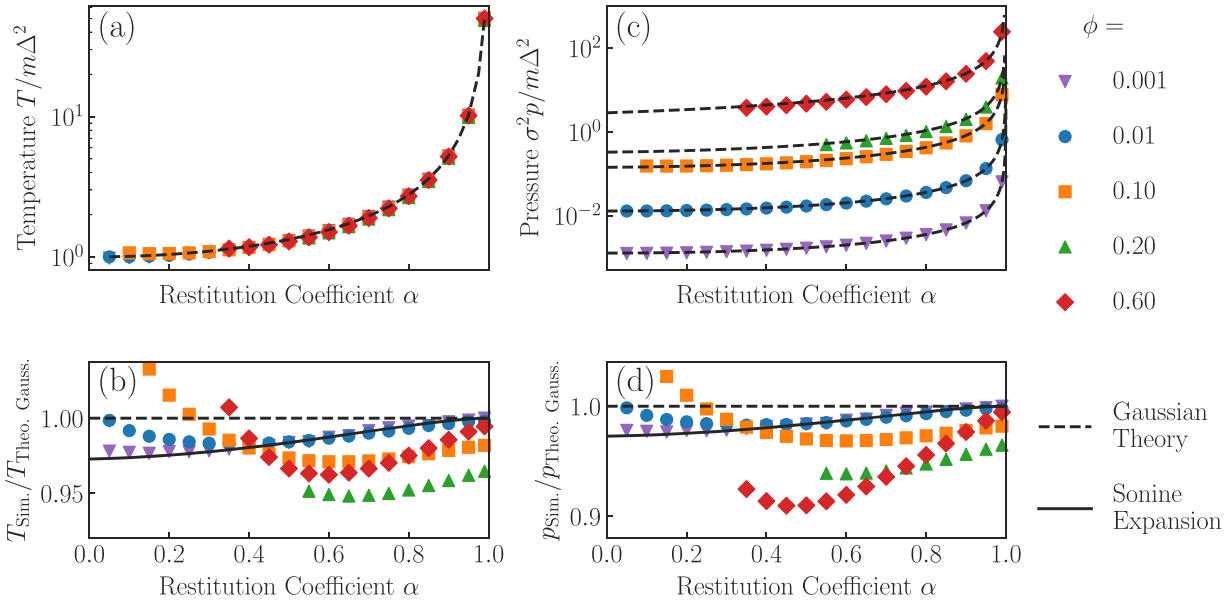

FIG. 5. Homogeneous temperature T [(a) and (b)] and pressure p [(c) and (d)] as functions of the restitution coefficient α for different values of the packing fraction ϕ. Panels (a) and (c) show the raw quantities, while panels (b) and (d) display the same data normalized by their Gaussian theoretical predictions [Eqs. (24) and (27) with T replaced by its Gaussian prediction]. Results are obtained for $N = 10^4$ particles, with each data point averaged over at least 10^3 independent snapshots. Only data corresponding to homogeneous configurations are shown; data exhibiting inhomogeneous states—typically occurring at large ϕ and low α and reminiscent of the nonuniform phase observed in Refs. 51, 54, 83, and 84—are omitted.

Here, we have used Eq. (3) to define $\mathbf{I}_{\alpha\beta}/m = -(1+\alpha)(\boldsymbol{v}_{\alpha\beta}\cdot\hat{\boldsymbol{\sigma}}_{\alpha\beta})\hat{\boldsymbol{\sigma}}_{\alpha\beta}/2 - \Delta\hat{\boldsymbol{\sigma}}_{\alpha\beta}^{\perp}$. Equations (25) and (26) yield an explicit expression for the homogeneous stress tensor $\boldsymbol{\Pi}^{\text{homo}}$ as a function of the model parameters (see the supplementary material),

$$\boldsymbol{\Pi}^{\text{homo}} = -p\boldsymbol{I} + \tau\boldsymbol{\varepsilon}, \tag{27a}$$

$$p = p^{\text{kinetic}} + p^{\text{coll}} = nT + n\phi\chi(1+\alpha)T, \tag{27b}$$

$$\tau = \tau^{\text{coll}} = n\phi\chi\sqrt{4\pi m T}\Delta. \tag{27c}$$

In this expression, the pressure reduces to the standard granular-gas result,[89] since the transverse chiral impulse does not contribute to the momentum transfer along the line connecting the particle centers, $\hat{\boldsymbol{\sigma}}$. By contrast, chirality generates a purely collisional torque density, τ, through the Δ term in the collision rule. The pressure includes an ideal-gas contribution of order $\mathcal{O}(n)$ from $m\boldsymbol{c}\otimes\boldsymbol{c}$, whereas τ is purely collisional, of order at least $\mathcal{O}(n^2)$, so that $|\tau| \ll p$ at low ϕ.

We compare simulations and theory in Figs. 5(c) and 5(d) by replacing T with its theoretical value [Eq. (24)]. The agreement is excellent, even though we use the equilibrium hard-disk estimate[82] $\chi \approx \chi^{\text{eq}} \simeq (1 - 7\phi/16 - \phi^3/20)/(1-\phi)^2$. An approximate Sonine correction is again proposed, where the temperature in Eq. (27) is replaced by the Sonine corrected one obtained in Appendix B. The comparison between numerical and theoretical results of τ [Eq. (27)] has already been shown in Fig. 2 and shows good agreement.

D. Chapman–Enskog ansatz

The hydrodynamic equations [Eqs. (4)] can be derived by taking time derivatives of the slow fields[96] (see Appendix C 1),

$$n(\mathbf{r},t) = \int f(\mathbf{r},\boldsymbol{v},t)d\boldsymbol{v}, \tag{28a}$$

$$\boldsymbol{u}(\mathbf{r},t) = \frac{1}{n(\mathbf{r},t)}\int \boldsymbol{v} f(\mathbf{r},\boldsymbol{v},t)d\boldsymbol{v}, \tag{28b}$$

$$T(\mathbf{r},t) = \frac{m}{2n(\mathbf{r},t)}\int (\boldsymbol{v}-\boldsymbol{u})^2 f(\mathbf{r},\boldsymbol{v},t)d\boldsymbol{v}. \tag{28c}$$

The homogeneous solution $f(\mathbf{r},\boldsymbol{v},t) = f(\boldsymbol{v})$ introduced above is independent of space and time and, therefore, cannot be used to derive hydrodynamic equations. To capture spatial and temporal variations, we construct an approximate solution of the Boltzmann equation through a suitable coarse-graining procedure using the Chapman–Enskog expansion. Originally developed to derive the Navier–Stokes equations for Hamiltonian systems[88] and subsequently extended in various directions,[60,96] this approach has more recently been applied to active matter,[97–106] including chiral models with simplified dynamics.[86]

The Chapman–Enskog method assumes that the space and time dependence of f enters only through the hydrodynamic fields and their gradients[96,107] so that we have

$$f(\mathbf{r},\boldsymbol{v},t) \equiv f[n(\mathbf{r},t),\boldsymbol{u}(\mathbf{r},t),T(\mathbf{r},t)|\boldsymbol{v}]. \tag{29}$$

15 July 2026 13:12:18

Published under an exclusive license by AIP Publishing

To proceed, we perform a gradient expansion on the Boltzmann equation [Eq. (14)] by introducing a bookkeeping parameter μ set back to 1 at the end of the calculation,

$$f = f^{(0)}(1 + \mu\Phi^{(1)} + \cdots), \qquad \nabla \to \mu\nabla. \tag{30}$$

In practice, the expansion is never performed beyond $\mathcal{O}(\mu^1) \sim \mathcal{O}(\nabla^1)$, because the resulting hydrodynamic equations are typically unstable.[108,109] This ansatz is expected to hold on timescales much longer than the mean time interval between collisions so that the dynamics is governed solely by the slow fields n, $\boldsymbol{u}$, and the quasi-slow field T. Here, $f^{(0)}$ corresponds to the previously obtained homogeneous solution—with density and temperature promoted to spatially varying fields—yielding the dissipationless Euler terms at order $\mathcal{O}(\nabla)$. The term $\Phi^{(1)}$ captures deviations from this local equilibrium through field gradients, supplying the $\mathcal{O}(\nabla^2)$ viscous and thermal-transport corrections that complete the chiral Navier–Stokes equations.[96] Regarding the values of the transport coefficients, we remark that this approach is fully consistent with the linear response one proposed in Ref. 58 (see also Ref. 86).

We will work in the dilute limit by assuming collisions occur at the same position $\mathbf{r}_1$ for both particles, rather than at $\mathbf{r}_1$ and $\mathbf{r}_2 = \mathbf{r}_1 - \sigma\hat{\boldsymbol{\sigma}}_{12}$. This yields

$$\mathcal{J}^{\text{dilute}}(\mathbf{r}_1, \boldsymbol{v}_1 | f, f) = \sigma\chi \int d\boldsymbol{v}_2 d\hat{\boldsymbol{\sigma}}_{12} \Theta(-\boldsymbol{v}_{12}\cdot\hat{\boldsymbol{\sigma}}_{12}) |\boldsymbol{v}_{12}\cdot\hat{\boldsymbol{\sigma}}_{12}| \times \left[\frac{f(\mathbf{r}_1, \boldsymbol{v}_1'') f(\mathbf{r}_1, \boldsymbol{v}_2'')}{\alpha^2} - f(\mathbf{r}_1, \boldsymbol{v}_1) f(\mathbf{r}_1, \boldsymbol{v}_2)\right], \tag{31}$$

which has to be compared with Eq. (18). This approximation neglects Enskog (collisional-transfer) contributions to the fluxes, retaining only the kinetic terms.[110,111] As a result, the stress reduces to its kinetic part and is symmetric by construction (see also Appendix C 1). It therefore cannot capture $\mathcal{O}(n^2)$ effects, such as the collisional torque density or any antisymmetric stress,

$$\boldsymbol{\Pi} = \boldsymbol{\Pi}^{\text{kin}} = -m \int \boldsymbol{c} \otimes \boldsymbol{c} f(\mathbf{r}, \boldsymbol{v}, t) d\boldsymbol{c}, \tag{32}$$

where $\boldsymbol{c} = \boldsymbol{v} - \boldsymbol{u}$ and $\Pi_{ij}^{\text{kin}} = \Pi_{ji}^{\text{kin}}$. While odd viscosity is included—since it contributes to the symmetric part of the stress—other parity-odd viscosities that produce a nonsymmetric stress cannot be captured.

Finally, due to momentum conservation, the transport coefficients in our two-dimensional fluid exhibit a logarithmic divergence with system size.[112,113] This effect is smaller than the numerical accuracy for the system sizes considered and is therefore neglected, as it lies beyond the scope of our non-fluctuating Chapman–Enskog approach, which yields the "bare" transport coefficients.

E. Order μ^0

At order μ^0, the Boltzmann equation [Eq. (14)] reduces to

$$\partial_t^{(0)} f^{(0)} = \mathcal{J}^{\text{dilute}}(f^{(0)}, f^{(0)}), \tag{33}$$

where $\partial_t^{(0)}$ denotes the $\mathcal{O}(\mu^0)$ part of the time derivative. Recalling that f is a function of the hydrodynamic fields, we obtain

$$\partial_t f^{(0)} = (\partial_t n)\partial_n f^{(0)} + (\partial_t \boldsymbol{u})\cdot\partial_{\boldsymbol{u}} f + (\partial_t T)\partial_T f. \tag{34}$$

From Eqs. (4), $\partial_t n$ and $\partial_t \boldsymbol{u}$ are $\mathcal{O}(\mu)$, as they involve gradients, whereas $\partial_t T = \delta\dot{T} + \mathcal{O}(\mu^1)$ is generally of order $\mathcal{O}(\mu^0)$. We assume, however, that collisions rapidly relax temperature fluctuations so that the temperature is locally steady, $\delta\dot{T}(\mathbf{r}) \simeq 0$, making T a fast field. Nonetheless, imposing $\partial_t T = 0$ at all orders leads to unphysical values of the viscosities. For this reason, we retain T as an independent hydrodynamic field with its own evolution equation, as is standard in granular hydrodynamics.[80] This approximation leads to $\partial_t^{(0)} f^{(0)} = 0$ and, therefore,

$$\mathcal{J}^{\text{dilute}}(f^{(0)}, f^{(0)}) = 0. \tag{35}$$

This equation is formally identical to the homogeneous one [Eq. (19)] and, therefore, admits the same solution. In particular, we have seen that a Gaussian provides an accurate approximation. However, the parameters entering $f^{(0)}$ do not necessarily coincide *a priori* with the hydrodynamic fields n, T, and $\boldsymbol{u}$, since these fields are defined by Eqs. (28) and can be influenced by $\Phi^{(1)}$. Nonetheless, the Chapman–Enskog approach assumes that $f^{(0)}$ is written in terms of the hydrodynamic fields themselves,[114,115]

$$f^{(0)}(\mathbf{r}, \boldsymbol{v}, t) = \frac{mn(\mathbf{r}, t)}{2\pi T(\mathbf{r}, t)} \exp\left[-\frac{m(\boldsymbol{v} - \boldsymbol{u}(\mathbf{r}, t))^2}{2T(\mathbf{r}, t)}\right], \tag{36}$$

with the parameters promoted to slowly varying fields. One may also include the previously discussed Sonine corrections to $f^{(0)}$, but their contribution is negligible.

F. Order μ^1: Generality

At order μ^1, Eq. (14) becomes[96]

$$\left(\partial_t^{(1)} + \boldsymbol{v}\cdot\nabla\right) f^{(0)} \equiv \mathcal{L}[\Phi^{(1)}], \tag{37}$$

where we defined $\mathcal{L}$ as the linear Boltzmann operator

$$\mathcal{L}[\Phi^{(1)}] = \mathcal{J}^{\text{dilute}}(f^{(0)}, f^{(0)}\Phi^{(1)}) + \mathcal{J}^{\text{dilute}}(f^{(0)}\Phi^{(1)}, f^{(0)}). \tag{38}$$

Using the $\mathcal{O}(\mu)$ hydrodynamic equations, we have

$$\begin{aligned} \partial_t^{(1)} n &= -\nabla\cdot(n\boldsymbol{u}), \\ \partial_t^{(1)} \boldsymbol{u} &= -(\boldsymbol{u}\cdot\nabla)\boldsymbol{u} + \frac{1}{mn}\nabla\cdot\boldsymbol{\Pi}^{\text{homo}}, \\ \partial_t^{(1)} T &= -\boldsymbol{u}\cdot\nabla T - T\nabla\cdot\boldsymbol{u}. \end{aligned} \tag{39}$$

In the dilute approximation, we neglect collisional transfer and, hence, also the torque and use $\boldsymbol{\Pi}^{\text{homo}} = -p\mathbf{1} = -nT\mathbf{1}$. Inserting Eq. (36) into Eq. (37) yields[60]

$$\left(\partial_t^{(1)} + \boldsymbol{v}\cdot\nabla\right) f^{(0)} = \frac{1}{T}(\mathbf{D}(\boldsymbol{c}) : \nabla\boldsymbol{u} + \mathbf{A}(\boldsymbol{c})\cdot\nabla\log T) f^{(0)}, \tag{40}$$

where $\boldsymbol{c} = \boldsymbol{v} - \boldsymbol{u}$ and

$$\mathbf{A}(\boldsymbol{c}) = \left(\frac{mc^2}{2} - 2T\right)\boldsymbol{c}, \quad \mathbf{D}(\boldsymbol{c}) = m\left(\boldsymbol{c}\otimes\boldsymbol{c} - \frac{c^2}{2}\mathbf{1}\right). \tag{41}$$

Substituting Eq. (40) into Eq. (37), we obtain the equation for $\Phi^{(1)}$,

$$\frac{f^{(0)}}{T}(\mathbf{D}(\boldsymbol{c}) : \nabla\boldsymbol{u} + \mathbf{A}(\boldsymbol{c})\cdot\nabla\log T) = \mathcal{L}[\Phi^{(1)}]. \tag{42}$$

15 July 2026 13:12:18

Published under an exclusive license by AIP Publishing

A formal solution of Eq. (42) requires a (pseudo-) inverse[115,116] of $\mathcal{L}$. Instead, guided by linearity and rotational invariance, we expand $\Phi^{(1)}$ in irreducible tensorial representations of $O(2)$, allowing for both even and odd two-dimensional tensors,[86]

$$\Phi^{(1)} = \left(\mathcal{D}(c^2)\mathbf{D} + \mathcal{D}^{\perp}(c^2)\mathbf{D}^{\perp}\right) : \nabla \boldsymbol{u} + \left(\mathcal{A}(c^2)\mathbf{A} + \mathcal{A}^{\perp}(c^2)\mathbf{A}^{\perp}\right) \cdot \nabla \log T, \tag{43}$$

where we have introduced $\mathbf{A}^{\perp} = \boldsymbol{\varepsilon} \cdot \mathbf{A}$ and $\mathbf{D}^{\perp} = \boldsymbol{\varepsilon} \cdot \mathbf{D}$, together with the unknown scalar functions $\mathcal{D}$, $\mathcal{D}^{\perp}$, $\mathcal{A}$, and $\mathcal{A}^{\perp}$. Although the left-hand side of Eq. (42) depends only on $\mathbf{D}$ and $\mathbf{A}$, chirality permits the operator $\mathcal{L}$ to mix these tensors with their transverse counterparts, coupling $\mathbf{D}$ to $\mathbf{D}^{\perp}$ and $\mathbf{A}$ to $\mathbf{A}^{\perp}$, in contrast to nonchiral systems.[58] This coupling underlies the emergence of nonzero odd transport coefficients. Since Eq. (42) contains no scalar coefficient on its left-hand side, $\Phi^{(1)}$ does not include any term proportional to $\nabla \cdot \boldsymbol{u}$, consistent with the vanishing bulk viscosity of dilute smooth monatomic gases.[88,117]

To proceed, we assume the unknown functions to be constants, namely $\mathcal{D}(c^2) = \mathcal{D}_0$, $\mathcal{D}^{\perp}(c^2) = \mathcal{D}_0^{\perp}$, $\mathcal{A}(c^2) = \mathcal{A}_0$, and $\mathcal{A}^{\perp}(c^2) = \mathcal{A}_0^{\perp}$. In principle, these functions could be expanded in a polynomial basis to retain their velocity dependence; however, higher-order terms are typically negligible.[88] By linearity and rotational invariance, $\mathcal{L}$ does not couple irreducible tensors of different rank, so each sector can be treated independently. We therefore first focus on the shear sector associated with $\mathbf{D}$ and $\mathbf{D}^{\perp}$.

G. Order μ^1: Obtaining $\mathcal{D}_0$ and $\mathcal{D}_0^{\perp}$

To determine $\mathcal{D}_0$ and $\mathcal{D}_0^{\perp}$, we introduce the matrix elements of the linearized collision operator

$$\mathsf{L}_{\alpha\beta} \equiv \left\langle \left(f^{(0)}\right)^{-1} D_{ij}^{(\alpha)}, \mathcal{L}[D_{ij}^{(\beta)}] \right\rangle, \quad \alpha, \beta \in \{\parallel, \perp\}, \tag{44}$$

with scalar product

$$\langle \psi, \phi \rangle \equiv \int f^{(0)}(\boldsymbol{c}) \psi(\boldsymbol{c}) \phi(\boldsymbol{c}) d\boldsymbol{c}, \tag{45}$$

and $D_{ij}^{(\parallel)} \equiv D_{ij}$, $D_{ij}^{(\perp)} \equiv D_{ij}^{\perp}$. Factoring out the velocity-gradient tensor, the shear part of Eq. (42) yields

$$\frac{f^{(0)}}{T}\mathbf{D}(\boldsymbol{c}) = \mathcal{D}_0 \mathcal{L}[\mathbf{D}(\boldsymbol{c})] + \mathcal{D}_0^{\perp} \mathcal{L}[\mathbf{D}^{\perp}(\boldsymbol{c})]. \tag{46}$$

By projecting onto the basis $\{D_{ij}, D_{ij}^{\perp}\}$, we obtain

$$\frac{1}{T}\begin{pmatrix} \langle D_{ij}, D_{ij} \rangle \\ \langle D_{ij}, D_{ij}^{\perp} \rangle \end{pmatrix} = \begin{pmatrix} \mathsf{L}_{\parallel\parallel} & \mathsf{L}_{\parallel\perp} \\ \mathsf{L}_{\perp\parallel} & \mathsf{L}_{\perp\perp} \end{pmatrix} \begin{pmatrix} \mathcal{D}_0 \\ \mathcal{D}_0^{\perp} \end{pmatrix}. \tag{47}$$

Rotational invariance implies $\mathsf{L}_{\perp\parallel} = -\mathsf{L}_{\parallel\perp}$ and $\mathsf{L}_{\perp\perp} = \mathsf{L}_{\parallel\parallel}$. In a parity-invariant system, $\mathcal{P}^{-1}\mathcal{L}\mathcal{P} = \mathcal{L}$ (with $\mathcal{P}$ the reflection operator) forbids mixing between $\mathbf{D}$ and $\mathbf{D}^{\perp}$; hence, $L_{\parallel\perp} = 0$ and parity-odd transport is excluded. Parity-odd transport, therefore, requires parity breaking[86] and hence a non-self-adjoint $\mathcal{L}$. However, $\mathcal{L}$ can be non-self-adjoint for many reasons unrelated to parity breaking, and non-self-adjointness alone does not guarantee odd transport: generic non-self-adjoint collision operators—such as those in equilibrium dense gases[118] or in dissipative dilute granular gases[119] ($\Delta = 0$)—do not, by themselves, generate parity-odd transport.

Using the relations $\langle D_{ij}, D_{ij} \rangle = 4nT^2$ and $\langle D_{ij}^{\perp}, D_{ij} \rangle = 0$, we find

$$\mathcal{D}_0 = 4nT \frac{\mathsf{L}_{\parallel\parallel}}{\mathsf{L}_{\parallel\parallel}^2 + \mathsf{L}_{\parallel\perp}^2}, \quad \mathcal{D}_0^{\perp} = 4nT \frac{\mathsf{L}_{\parallel\perp}}{\mathsf{L}_{\parallel\parallel}^2 + \mathsf{L}_{\parallel\perp}^2}. \tag{48}$$

The evaluation of $\mathbf{L}$ is straightforward but lengthy (see Appendix C 3 for details) and leads to the following result:

$$\begin{aligned} \mathsf{L}_{\parallel\parallel} &= -\chi\sigma n^2 T^2 \sqrt{\frac{\pi T}{m}}\left(\frac{m\Delta^2}{T} + (1+\alpha)(7-3\alpha)\right) \\ &= -4\sqrt{\pi}\chi\sigma n^2 m^2 |\Delta|^5 \frac{(2-\alpha)(1+\alpha)}{(1-\alpha^2)^{5/2}}, \end{aligned} \tag{49}$$

$$\begin{aligned} \mathsf{L}_{\parallel\perp} &= 2\pi\chi\sigma n^2 T^2 \Delta(1-\alpha) \\ &= 2\pi\chi\sigma n^2 m^2 \Delta^5 \frac{1}{(1-\alpha)(1+\alpha)^2}. \end{aligned} \tag{50}$$

In both cases, the second line is obtained by substituting the steady-state temperature [Eq. (24)]. We nevertheless keep T, Δ, and α explicit in the intermediate expressions. Treating them as independent is unphysical but useful for building intuition and for consistency checks in various limits, as we now do.

At fixed T, the achiral limit $\Delta \to 0$ restores parity, so the cross coefficient vanishes: $\mathsf{L}_{\parallel\perp} \to 0$. The longitudinal coefficient $\mathsf{L}_{\parallel\parallel}$ also goes to zero, but only once T is replaced by its steady-state value, since $T \to 0$ as $\Delta \to 0$. If instead one sets $\Delta = 0$ while keeping T and α fixed, the term $\mathsf{L}_{\parallel\parallel}$ remains finite, formally recovering the dissipative hard-disk result[60] and, as $\alpha \to 1$, the equilibrium hard-disk limit.[88]

The limit $\alpha \to 1$ is singular because $T \to \infty$. Substituting the steady-state temperature therefore causes L to diverge. At fixed T, however, $\mathsf{L}_{\parallel\perp} \propto 1 - \alpha$, so $\mathsf{L}_{\parallel\perp}$ remains nonzero near $\alpha = 1$ only due to the divergence of T. Without this divergence, the coefficient would vanish even when parity is broken by Δ. This surprising result originates from the microscopic collision rules: chirality allows a single collision to rotate D into $D^{\perp}$. Yet, in the limit $\alpha \to 1$, each such contribution is canceled by its mirror counterpart in the relevant integrals. Dissipation lifts this cancellation because $\boldsymbol{v}_{12}' \cdot \hat{\boldsymbol{\sigma}}_{12} \neq -\boldsymbol{v}_{12} \cdot \hat{\boldsymbol{\sigma}}_{12}$, thereby leaving a finite coupling $\mathsf{L}_{\parallel\perp} \propto \Delta(1-\alpha)$.

With $\mathcal{D}_0$ and $\mathcal{D}_0^{\perp}$ in hand, we can now compute the viscosities.

H. Order μ^1: The viscosities

With Eq. (32) and $f = f^{(0)}(1 + \mu\Phi^{(1)})$, the stress splits into a zeroth-order (homogeneous) part and a first-order (viscous) correction,

$$\begin{aligned} \boldsymbol{\Pi} &= -m \int \boldsymbol{c} \otimes \boldsymbol{c} f^{(0)}(1 + \mu\Phi^{(1)}) d\boldsymbol{c} \\ &= -nT\mathbf{1} - \mu m \int \boldsymbol{c} \otimes \boldsymbol{c} f^{(0)} \Phi^{(1)} d\boldsymbol{c}. \end{aligned} \tag{51}$$

Substituting $\Phi^{(1)}$ [Eq. (43)] into Eq. (51), we obtain

$$\Pi_{ij}^{\text{viscous}} = -\left(m\mathcal{D}_0 \int f^{(0)} c_i c_j D_{kl} d\boldsymbol{c}\right)\partial_k u_l - \left(m\mathcal{D}_0^{\perp} \int f^{(0)} c_i c_j D_{kl}^{\perp} d\boldsymbol{c}\right)\partial_k u_l$$

15 July 2026 13:12:18

Published under an exclusive license by AIP Publishing

$$= -nT^2\mathcal{D}_0(\delta_{ik}\delta_{jl} + \delta_{il}\delta_{jk} - \delta_{ij}\delta_{kl})\partial_k u_l + nT^2\mathcal{D}_0^{\perp}(\varepsilon_{ik}\delta_{jl} + \varepsilon_{jl}\delta_{ik})\partial_k u_l, \quad (52)$$

which, upon identification with the viscosity tensor [Eq. (8)], yields

$$\eta_s = -nT^2\mathcal{D}_0, \quad \eta_o = nT^2\mathcal{D}_0^{\perp}, \quad \zeta = \eta_A = \eta_B = \eta_R = 0. \quad (53)$$

We note that the primary effect of chirality is to generate an odd viscosity η_o. By contrast, the antisymmetric viscosities η_A and η_R vanish because the kinetic stress is symmetric, while ζ and η_B are zero since $\Phi^{(1)}$ contains no scalar $\nabla \cdot \boldsymbol{u}$ sectors. However, these coefficients are expected to acquire collisional contributions in the non-dilute limit.

Using Eqs. (48), (50), and (53), we finally obtain

$$\eta_s = \frac{4m|\Delta|(2-\alpha)}{\chi\sigma\sqrt{\pi}\sqrt{1-\alpha^2}P(\alpha)}, \quad (54a)$$

$$\eta_o = \frac{2m\Delta(1-\alpha)}{\chi\sigma(1+\alpha)P(\alpha)}, \quad (54b)$$

with $P(\alpha)$ a positive polynomial in $0 \le \alpha \le 1$,

$$P(\alpha) = 4(2-\alpha)^2(1+\alpha) + \pi(1-\alpha)^3. \quad (55)$$

We note that the viscosity η_s can be rewritten as

$$\eta_s = \frac{4(2-\alpha)}{\chi\sigma P(\alpha)}\sqrt{\frac{mT_{\text{Gauss}}}{\pi}}, \quad (56)$$

upon substituting T_{Gauss} [Eq. (24)] into Eq. (54a). This compact expression shows that chirality (through Δ) primarily renormalizes the conventional viscosity η_s via the temperature T_{Gauss}. Moreover, in the elastic limit $\alpha \to 1$ ($P(\alpha \to 1) = 8$), it reproduces the standard equilibrium result for the viscosity of a hard-disk gas.[88]

Figure 6(a) compares simulations with Eq. (54) for the shear viscosity, showing excellent agreement at low ϕ. Theory and simulations for η_o were already compared in Fig. 3(a); as noted there, $\eta_o \to 0$ as $\alpha \to 1$. This indicates that, in this model, odd viscosity requires dissipative normal collisions. Indeed, in the limit $\alpha \to 1$, the temperature diverges so that $m\Delta^2/T \sim 1-\alpha^2 \to 0$. As a result, chirality becomes asymptotically negligible and $\lfloor_{\parallel\perp}/\lfloor_{\parallel\parallel} \to 0$ [Eqs. (50)], causing η_o to vanish. An alternative argument can be made at fixed T; in that case, $\lfloor_{\parallel\perp} \propto T^2\Delta(1-\alpha)$, which directly implies $\eta_o \propto 1-\alpha$ [Eq. (C20)]. However, with this model, the divergence of T as $\alpha \to 1$ masks this effect, and the vanishing of the odd viscosity has to be found in the previous argument. This mechanism becomes relevant when T remains finite as $\alpha \to 1$, for example, because of external damping. We return to this point in the conclusion.

I. Order μ^1: The thermal conductivities

Applying the same Chapman–Enskog procedure in the thermal sector yields the regular and odd thermal conductivities, κ and κ_o. As detailed in Appendix C 4,

$$\kappa = \frac{16|\Delta|(1+\alpha)(4-3\alpha)}{\chi\sigma\sqrt{\pi}\sqrt{1-\alpha^2}Q(\alpha)}, \quad (57a)$$

$$\kappa_o = \frac{8\Delta(1-\alpha)}{\chi\sigma Q(\alpha)}, \quad (57b)$$

where Q is a positive polynomial given in Appendix C 4. As for viscosity, chirality generates the odd conductivity κ_o and affects the conventional conductivity κ. In the elastic limit $\alpha \to 1$, κ diverges due to the divergence of the steady-state temperature, while $\kappa_o \to 0$. Figures 6(b) and 3(b) show good agreement with simulations at low ϕ. The small discrepancies between the theory and simulations for the odd thermal conductivity are likely attributable to the

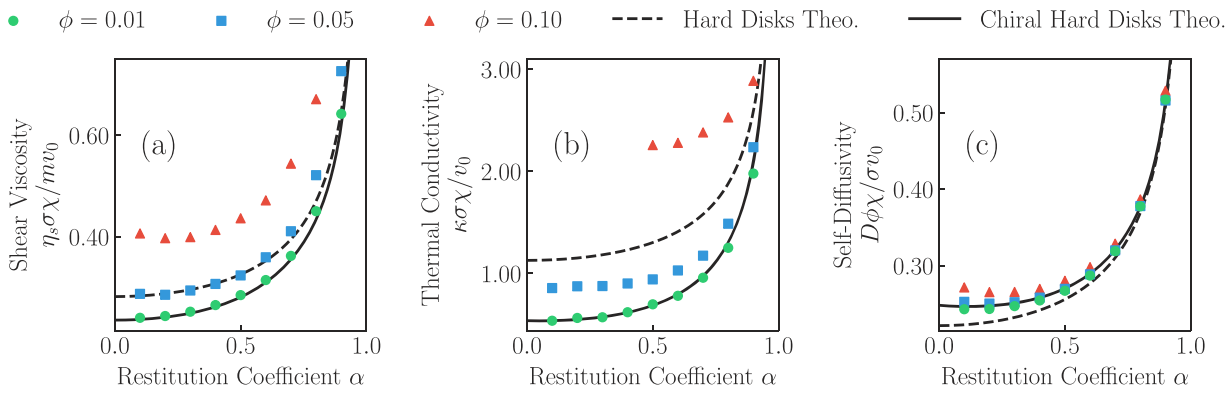

FIG. 6. Even transport coefficients as functions of the restitution coefficient α at several densities ϕ. (a) Shear viscosity measured from an imposed shear flow, as detailed in Appendix A 2. (b) Thermal conductivity measured by imposing a temperature gradient via a spatially dependent driving $\Delta = \Delta(x)$, as discussed in Appendix A 3. The missing data points for $\phi = 0.1$ correspond to systems in which the smallest numerically accessible thermal gradient was still too large to yield reliable measurements. (c) Self-diffusivity measured using a Green–Kubo relation (see Appendix A 4 for details). Solid lines show the predictions of the chiral theory [Eqs. (54), (57), and (59)], while dashed lines indicate the expected values for regular hard disks at equilibrium temperature $k_B T^{\text{eq}} = m\Delta^2/(1-\alpha^2)$. The parameter v_0 denotes an arbitrary reference velocity, kept fixed across simulations to allow a direct comparison between the chiral and equilibrium cases without rescaling by the temperature, which provides the only natural velocity scale at equilibrium but varies with α in our system.

15 July 2026 13:12:18

Published under an exclusive license by AIP Publishing

difficulties in measuring this transport coefficient, as explained in Appendix A 3.

By substituting the temperature $T_{\rm Gauss}$ [Eq. (24)] into Eq. (C28), we obtain a compact expression for the thermal conductivity,

$$\kappa = \frac{16(1+\alpha)(4-3\alpha)}{\chi\sigma Q(\alpha)}\sqrt{\frac{T_{\rm Gauss}}{\pi m}}. \tag{58}$$

In the elastic limit $\alpha \to 1$ ($Q(\alpha \to 1) = 16$), this expression reduces to the results for a dilute hard-disk gas.[88] It shows that chirality (through Δ) primarily affects the thermal conductivity κ by renormalizing it via the temperature $T_{\rm Gauss}$.

J. Self-diffusivities via Chapman–Enskog

The self-diffusivity D and its odd counterpart D_o follow from a Chapman–Enskog expansion of the Boltzmann–Lorentz equation for a tagged particle.[60] In this framework, the nonlinear bilinear operator $\mathcal{J}(\mathbf{r},\boldsymbol{v}|f,f)$ is replaced by the linear tracer-bath operator $\mathcal{J}(\mathbf{r},\boldsymbol{v}|f_s,f_B)$, where only the tracer distribution f_s evolves and "collides" with the bath distribution $f_B \equiv f^{(0)}(\boldsymbol{v})$.

Performing a Chapman–Enskog expansion on f_s, we obtain the self-diffusivities[120] (see Appendix C 5 for the derivation),

$$D = \frac{\sqrt{\pi}\sigma|\Delta|}{\phi\chi\sqrt{1-\alpha^2}R(\alpha)}, \tag{59a}$$

$$D_o = \frac{\pi\sigma\Delta}{2\phi\chi(1+\alpha)R(\alpha)}, \tag{59b}$$

with $R(\alpha)$ a strictly positive polynomial given in Appendix C 5.

As in the case of viscosity (η_s) and thermal conductivity (κ), chirality introduces off-diagonal antisymmetric elements in the diffusion matrix (odd diffusivity D_o) and renormalizes the diagonal self-diffusivity D through the temperature $T_{\rm Gauss}$ [Eq. (24)]. By substituting Eq. (24) into Eq. (59a), the self-diffusivity can be expressed as

$$D = \frac{4}{n\chi\sigma R(\alpha)}\sqrt{\frac{T_{\rm Gauss}}{\pi m}}. \tag{60}$$

As expected, this compact expression shows that D reduces to the standard hard-disk result[60] in the elastic limit $\alpha \to 1$, for which $R(\alpha \to 1) = 8$.

As a consequence of the temperature divergence in the elastic limit, the self-diffusion D diverges, while D_o remains finite as $\alpha \to 1$. Indeed, each chiral collision imparts an oriented transverse kick to the tagged particle, so the mean transverse response—and the corresponding integrals—remain finite even as $\alpha \to 1$. However, as for odd viscosity and odd conductivity, the ratio of off-diagonal to diagonal matrix elements of the linearized Boltzmann–Lorentz operator still vanishes in this limit. The comparison between simulations and theory shows excellent agreement across a broad range of densities within the low-density regime, as illustrated in Figs. 6(c) and 3(c). At higher packing fractions, however, both the odd and even self-diffusion coefficients tend to increase slightly.

Although the self-diffusivity is well defined, the system as a whole does not diffuse in the absence of an external bath. A natural extension would therefore be to add noise and study how the collective diffusivity depends on the packing fraction. In the strongly chiral regime, this dependence was recently found to be non-monotonic,[121] as for the self-diffusion of active chiral tracers in passive baths.[122]

V. DISCUSSION AND OUTLOOK

Because our model is based on hard disks, the interaction is singular. Nevertheless, we expect the qualitative phenomenology derived here to persist for chiral fluids with short-ranged forces. In particular, systems with softer repulsive cores and short-ranged chiral interactions should display comparable behavior.[51] Indeed, one may start from a smooth N-particle dynamics, write a Liouville equation for the full phase-space distribution, and derive a Boltzmann description by truncating the associated BBGKY hierarchy.[50]

It is also straightforward to incorporate damping γ, possibly together with a Langevin bath at temperature T_b. Between collisions, the velocities would obey $\dot{\boldsymbol{v}} = -\gamma\boldsymbol{v} + \sqrt{2\gamma T_b/m}\boldsymbol{\zeta}(t)$ so that the Boltzmann equation acquires the additional contribution $\gamma\partial_{\boldsymbol{v}}\cdot(\boldsymbol{v}f) + \gamma T_b/m\partial^2_{\boldsymbol{v}}f$. Within the Chapman–Enskog expansion for a Gaussian homogeneous solution, this modification amounts to a simple shift of the linearized operator $\mathcal{L}[\bullet] \to \mathcal{L}[\bullet] + \gamma\partial_{\boldsymbol{v}}\cdot(\boldsymbol{v}\bullet) + \gamma T_b/m\partial^2_{\boldsymbol{v}}(\bullet)$. These new terms mainly change the steady-state temperature and shift the diagonal matrix elements of $\mathcal{L}$ after integration by parts.[123] In the shear sector, for instance, $\lfloor_{\parallel\parallel} \to \lfloor_{\parallel\parallel} - 8\gamma nT^2$ while $\lfloor_{\parallel\perp}$ is unchanged and the viscosities still follow from Eq. (53). Here T is determined from Eq. (22) as a stable positive root of the cubic equation:[94] $0 = \omega(\phi,T)\langle\delta E\rangle_{\rm coll}/2 - 2\gamma(T-T_b)$.

A limitation of our current computation is the dilute-gas approximation. It neglects collisional-transfer contributions to transport and, crucially, cannot capture antisymmetric stresses generated by collisions at finite densities. Yet this is precisely the experimentally relevant regime for most chiral systems such as crowded biological media.[7,124–126] Extending the theory beyond the dilute limit is thus essential to bridge this gap and identify the mechanisms that control dense chiral transport. Notably, it would lead to the first analytical expressions for the other odd transport coefficients, such as η_A or η_R.

The dense regime is also where correlations and fluctuations become unavoidable, motivating a fluctuating kinetic description beyond the Boltzmann–Grad limit: a fluctuating Boltzmann equation.[96,127,128] Non-Gaussian corrections to the velocity distribution captured by the Sonine expansion are known to violate the fluctuation–dissipation relation for the associated noise in the fluctuating Boltzmann equation and to induce memory effects in the hydrodynamic noise.[129,130] We expect these corrections to strongly influence the fluctuating hydrodynamics of chiral particles.[66]

Beyond fluids, in dense regimes, chirality can also produce an antisymmetric elastic response known as odd elasticity in amorphous or crystalline materials.[131] In equilibrium, hard-disk systems can be systematically coarse-grained to derive a hydrodynamic description of a crystal.[132] Carrying out an analogous program for active chiral crystals would be particularly timely, as these systems display a rich set of instabilities that depend sensitively on transport coefficients and elastic moduli.[56]

More broadly, while we focused on the self-diffusivity of a tagged particle identical to the bath constituents, an immediate

15 July 2026 13:12:18

Published under an exclusive license by AIP Publishing

extension is to consider a geometrically complex tracer immersed in a bath of chiral colliders.[133–137] By tuning the tracer shape, one can implement symmetry breaking in a controlled way and generate a hierarchy of nonequilibrium transport effects, from granular-ratchet drift[133,134] to autonomous rotation.[135,136]

Finally, extending these calculations to 3D is natural, but the symmetry constraints are qualitatively different from 2D.[41,138] In a fully isotropic 3D fluid, an odd viscosity is forbidden—no fourth-rank isotropic tensor can be built from a single ε_{ijk}—and the torque density $\tau_k = \varepsilon_{kij}\Pi_{ij}/2$ is a pseudovector that must vanish by isotropy. Odd viscosity and a nonzero $\boldsymbol{\tau}$ become possible only if isotropy is broken by a distinguished axis $\hat{\boldsymbol{\ell}}$ (e.g., selecting the plane of transverse kicks Δ), in which case one may write $\eta^{\rm odd}_{ijkl} = \eta_o\left(\varepsilon_{ikm}\hat{\ell}_m\delta_{jl} + \varepsilon_{jkm}\hat{\ell}_m\delta_{il}\right)$ and $\boldsymbol{\tau} = \tau\hat{\boldsymbol{\ell}}$. In principle, the additional contractions enabled by $\hat{\boldsymbol{\ell}}$ even allow for a richer set of transport coefficients than in 2D.

SUPPLEMENTARY MATERIAL

A Python notebook is provided as supplementary material to automatically evaluate all integrals encountered in this work.

ACKNOWLEDGMENTS

L.C. acknowledges financial support from the University of Rome Sapienza under the project Ateneo 2024 (Grant No. RM124190C54BE48D), "Elementary excitations at the origin of glassy or hexatic behavior in low dimensional system, at and out of equilibrium."

AUTHOR DECLARATIONS

Conflict of Interest

The authors have no conflicts to disclose.

Author Contributions

Raphaël Maire: Data curation (lead); Investigation (lead); Writing – original draft (lead); Writing – review & editing (equal). **Alessandro Petrini**: Investigation (equal); Writing – review & editing (equal). **Umberto Marini Bettolo Marconi**: Investigation (equal); Writing – review & editing (equal). **Lorenzo Caprini**: Conceptualization (lead); Investigation (equal); Writing – original draft (equal); Writing – review & editing (equal).

DATA AVAILABILITY

The data that support the findings of this study are available from the corresponding authors upon reasonable request.

APPENDIX A: NUMERICAL MEASUREMENT OF TRANSPORT COEFFICIENTS

1. Stress and heat current in event-driven molecular dynamics

The stress and heat current are generically given by a kinetic part plus an impulsive collisional contribution. For hard-disks with instantaneous collisions, their microscopic expressions read[139]

$$\begin{aligned}\boldsymbol{\Pi}(t) &= -\frac{m}{L^2}\sum_{\alpha=1}^{N}\boldsymbol{c}_\alpha(t)\otimes\boldsymbol{c}_\alpha(t) \\ &\quad + \frac{\sigma}{L^2}\sum_{\alpha<\beta}\hat{\boldsymbol{\sigma}}_{\alpha\beta}(t)\otimes\mathbf{I}_{\alpha\beta}(t)\delta\left(t-t^{\rm coll}_{\alpha\beta}\right), \\ \boldsymbol{J}(t) &= +\frac{m}{2L^2}\sum_{\alpha=1}^{N}\boldsymbol{c}_\alpha^2(t)\boldsymbol{c}_\alpha(t) \\ &\quad - \frac{\sigma}{L^2}\sum_{\alpha<\beta}\left[\mathbf{I}_{\alpha\beta}(t)\cdot\boldsymbol{C}_{\alpha\beta}(t)\right]\hat{\boldsymbol{\sigma}}_{\alpha\beta}(t)\delta\left(t-t^{\rm coll}_{\alpha\beta}\right),\end{aligned} \tag{A1}$$

where $\boldsymbol{c}_\alpha = \boldsymbol{v}_\alpha - \langle\boldsymbol{v}\rangle$, $\boldsymbol{C}_{\alpha\beta} = (\boldsymbol{c}_\alpha + \boldsymbol{c}_\beta)/2$, and $\mathbf{I}_{\alpha\beta}$ is the impulse transferred during the collision between $\alpha\beta$, $\mathbf{I}_{\alpha\beta} \equiv m\left(\boldsymbol{v}'_\alpha - \boldsymbol{v}_\alpha\right) = -m\left(\boldsymbol{v}'_\beta - \boldsymbol{v}_\beta\right)$.

Transport coefficients are often expressed through Green–Kubo formulas with time integrals of current autocorrelations. However, the instantaneous microscopic currents contain impulsive collisional contributions, which would never be sampled via instantaneous measurement in the simulations, and only the kinetic term would be retained. Moreover, in driven, nonequilibrium steady states, Green–Kubo relations are not guaranteed to hold in their equilibrium form.[140] We therefore avoid this route whenever an alternative, more direct evaluation is available.

2. Viscosities

The viscosities are measured under a controlled simple shear rate $\dot{\gamma}$ imposed via Lees–Edwards boundary conditions[141] in a box of size $L_x \times L_y$ where the periodic images above and below the simulation cell slide along $\hat{x}$ with velocities $\pm\dot{\gamma}L_y/2$ (equivalently, a relative velocity $\dot{\gamma}L_y$ between the top and bottom images). This introduces a time-dependent shear offset $\delta x(t) = \dot{\gamma}tL_y$ between adjacent replicas. Accordingly, when a particle crosses the top or bottom boundary, its position is remapped as $y \to y \mp L_y$ together with an affine shift $x \to x \mp \delta x(t) \pmod{L_x}$.

Following Eqs. (4), such boundary conditions impose a shear profile

$$\boldsymbol{u}(y) = \dot{\gamma}y\hat{\boldsymbol{x}}, \tag{A2}$$

which implies

$$\partial_y u_x = \dot{\gamma}, \quad \partial_x u_x = \partial_x u_y = \partial_y u_y = 0. \tag{A3}$$

Using Eq. (7), we find

$$\eta_s = \frac{\langle\Pi_{xy} + \Pi_{yx}\rangle}{2\dot{\gamma}}, \qquad \eta_o = \frac{\langle\Pi_{xx} - \Pi_{yy}\rangle}{2\dot{\gamma}}. \tag{A4}$$

Since $\langle\Pi\rangle$ can be computed using a time average, the singular contributions of the collisions to the *instantaneous* stress are smoothed out to simple jumps in values.[142]

A drawback of this approach is that the range of $\dot{\gamma}$ over which the response is truly linear is not known *a priori*. In practice, we had to use an extremely low shear rate, $\sigma\dot{\gamma}/\Delta = 2 \times 10^{-6}$, because at larger values we observed a pronounced $\dot{\gamma}$ dependence of η_o. Beyond genuine nonlinearities, this sensitivity may also reflect the fact that even a nonchiral fluid under shear develops a nonzero normal-stress difference $\Pi_{xx} - \Pi_{yy}$. This term is typically neglected since in linear theories it appears only at Burnett order,[143] $\mathcal{O}(\nabla^3)$, but the

15 July 2026 13:12:18

Published under an exclusive license by AIP Publishing

small magnitude of η_o (despite entering already at Navier–Stokes order) likely makes it comparable to this Burnett-level contribution unless $\dot{\gamma}$ is taken extremely small. We note that η_s could be accurately measured with $\sigma\dot{\gamma}/\Delta \sim \mathcal{O}(10^{-3})$ for all our densities.

The viscosities are measured in systems of $N = 1000$ particles for a time $1.3 \times 10^9 \leq t\Delta/\sigma \leq 5 \times 10^9$ with between 5 and 50 independent realizations.

3. Conductivities

It is possible to measure the thermal conductivities by imposing a thermal gradient. However, a gradient generated by fixing T at two slabs (e.g., via a Müller–Plathe scheme[144]) is screened by bulk relaxation due to energy non-conservation during collision. Therefore, it is easier to impose the thermal gradient by directly fixing the temperature $T(x) \simeq m\Delta^2(x)/(1-\alpha^2)$ at each point by varying Δ with x. For example, we can ask that the temperature profile have a triangular shape: $T(x) = T_0 + \delta T/2 - 2\delta T|x - L_x/2|/L_x$ which linearly interpolates between $T(0) = T(L_x) = T_0 - \delta T/2$ and $T(L_x/2) = T_0 + \delta T/2$. Such a profile is imposed by using a collision rule dependent on the positions of the two particles, 1 and 2, with $\Delta_{12} = \sqrt{T(\,(x_1+x_2)/2\,)(1-\alpha^2)/m}$. Assuming δT to be small enough, $\partial_x T|_{x\simeq L_x/4} = -\partial_x T|_{x\simeq 3L_x/4} = \text{cst}$ and the conductivities can be obtained by measuring the local heat current around these points. This method works well for the regular thermal conductivity, but not for its odd counterpart. Indeed, the largest δT we can use while maintaining an acceptable signal-to-noise ratio still does not yield a converged value, as a slight increase in δT changes the extracted odd conductivity. One possible reason is that, under periodic boundary conditions, imposing a temperature gradient while enforcing $u_x = 0$ can generate a density gradient through the requirement of mechanical equilibrium (uniform pressure). This may contaminate the measurement because the resulting torque density may not remain uniform and can therefore induce a transverse flow ($u_y \neq 0$). In addition, if we retained Sonine corrections to the local stationary distribution so that $f^{(0)}$ were not strictly Gaussian, the heat current would acquire an additional contribution proportional to the density gradient,[110]

$$\boldsymbol{J}^{\text{non-Gaussian}} = -\lambda\nabla n - \lambda_o \boldsymbol{\varepsilon}\cdot\nabla n, \tag{A5}$$

which would further interfere with our determination of the thermal conductivity. For these reasons, we adopt an alternative method to measure this coefficient.

As previously described, the measurement of the instantaneous heat current is impossible for discontinuous potentials due to the singular terms arising in its expression. The typical method to circumvent this problem involves the use of Helfand moments[145] related to the time integral of J, which smooths out the singular contributions. However, no Helfand relation is available for the odd thermal conductivity, and we have to rely on the standard Green–Kubo expression[146]

$$\kappa_o = \frac{L^2}{2T^2}\int_0^\infty \langle J_x(t)J_y(0) - J_y(t)J_x(0)\rangle dt. \tag{A6}$$

In practice, since $\boldsymbol{J}(t)$ contains impulsive contributions, we evaluate the correlator using the time-averaged current over a finite small bin Δt, $\bar{\boldsymbol{J}}(t) = \Delta t^{-1}\int_t^{t+\Delta t}\boldsymbol{J}(t')dt'$, and compute Eq. (A6) with $\boldsymbol{J}\to\bar{\boldsymbol{J}}$. This binning is less problematic for κ_o than for κ (if we were to use a standard Green–Kubo for the latter), since the singular term[147] $\langle J_i(t)J_j(0)\rangle \propto \delta(0)$ cancels under antisymmetrization.

We see systematic discrepancies between the measurements and the theory for the thermal conductivities. Such discrepancies also appeared when we tried to evaluate the viscosities using Green–Kubo relations (with or without using Helfand moments). We also verified that no such strong discrepancies appeared in pure equilibrium hard disks for the regular thermal conductivity. This suggests that the issue is not the treatment of impulsive currents *per se*, but rather the limited applicability of equilibrium Green–Kubo relations in this nonequilibrium steady state.[140,148] We also note that using $n\langle|T(\boldsymbol{q}\to 0)|^2\rangle$ instead of T^2 [with $T(\boldsymbol{q})$ the Fourier transform of $T(\mathbf{r})$] in the denominator, as suggested by Ref. 146, does not improve the result.

The regular thermal conductivity is measured in systems with $\delta T/m\Delta^2 = 2\times 10^{-3}$, $N = 10\,000$, and $L_x = 3L_y$ for a time $2.5\times 10^8 \leq t\Delta/\sigma \leq 4\times 10^8$.

The odd thermal conductivity is measured in systems of $N = 2000$ particles where the autocorrelations are computed each $dt\Delta/\sigma = 1$ over a window of $t\Delta/\sigma = 2\times 10^6$ and averaged over ten independent realizations.

4. Self-diffusivities

The ordinary and odd self-diffusivities are obtained from the velocity-displacement correlations introduced in Ref. 29,

$$\begin{aligned} D &= \lim_{t\to\infty}\frac{\langle(x(t)-x(0))v_x(0) + (y(t)-y(0))v_y(0)\rangle}{2},\\ D_o &= \lim_{t\to\infty}\frac{\langle(x(t)-x(0))v_y(0) - (y(t)-y(0))v_x(0)\rangle}{2}. \end{aligned} \tag{A7}$$

Unlike stress or heat current autocorrelations in hard-particle systems, these estimators are free of impulsive singularities and can be evaluated directly without special regularization.

The diffusivities are measured in systems of $N = 200$ particles where the autocorrelations are computed each $dt\Delta/\sigma = 10$ over a window of $t\Delta/\sigma = 0.5\times 10^9$ and averaged over ten independent realizations.

APPENDIX B: SONINE EXPANSION FOR THE HOMOGENEOUS SOLUTION

The homogeneous distribution $f(\boldsymbol{v})$ must be obtained from the stationary Boltzmann equation

$$\mathcal{J}(\boldsymbol{v}|f,f) = 0. \tag{B1}$$

Using Eq. (18), the stationarity condition $\mathcal{J}(\boldsymbol{v}|f,f) = 0$ follows from a global balance between loss and gain terms. It is easier to check for the more restrictive pointwise (effective) detailed balance,

$$f(\boldsymbol{v}_1'')f(\boldsymbol{v}_2'') = \alpha^2 f(\boldsymbol{v}_1)f(\boldsymbol{v}_2). \tag{B2}$$

At equilibrium, $\alpha\to 1$ and $\Delta\to 0$; such a relation is *exactly* satisfied by a Gaussian. We can try to see how far away we are from the Gaussian in our case,

15 July 2026 13:12:18

Published under an exclusive license by AIP Publishing

$$\alpha^2 \frac{f^G(\boldsymbol{v}_1) f^G(\boldsymbol{v}_2)}{f^G(\boldsymbol{v}_1'') f^G(\boldsymbol{v}_2'')} = \alpha^2 \exp\left(\frac{\boldsymbol{v}_1''^2 + \boldsymbol{v}_2''^2 - \boldsymbol{v}_1^2 - \boldsymbol{v}_2^2}{2T/m} \right)$$
$$= \alpha^2 \exp\left(\frac{(\alpha^{-2} - 1)(\boldsymbol{v}_{12} \cdot \hat{\boldsymbol{\sigma}}_{12})^2}{2T/m} + \frac{2\Delta^2 + 2\Delta \boldsymbol{v}_{12} \cdot \hat{\boldsymbol{\sigma}}_{12}^{\perp}}{2T/m} \right). \quad \text{(B3)}$$

The right-hand side must approach 1 if a Gaussian is a solution. In the limit $\alpha \to 1$ and $\Delta \to 0$, since collisions conserve energy, the Gaussian is exactly a solution. In the case $\alpha \neq 1$ and $\Delta \neq 0$, a Gaussian typically does not satisfy Eq. (B1). However, we saw that $T = m\Delta^2/(1-\alpha^2)$ and since $\boldsymbol{v}_{12} \sim \mathcal{O}(\sqrt{T})$, the two terms proportional to Δ and Δ^2 become negligible in the limit $\alpha \to 1$ since $T \propto (1-\alpha^2)^{-1} \to \infty$. Similarly, the term proportional to $\alpha^{-2} - 1$ vanishes in this limit, leaving

$$\lim_{\alpha \to 1} \alpha^{-2} \frac{f^G(\boldsymbol{v}_1'') f^G(\boldsymbol{v}_2'')}{f^G(\boldsymbol{v}_1) f^G(\boldsymbol{v}_2)} = 1. \quad \text{(B4)}$$

Therefore, a Gaussian is a solution in the limit $\alpha \to 1$ because the energy increments of Δ at collision are negligible with respect to the system temperature T.

We now compute perturbative corrections to f^G around $\alpha \to 1$ using a Sonine expansion[60]

$$f(\boldsymbol{v}) = f^G(\boldsymbol{v}) \left(1 + a_1 S_1(\boldsymbol{v}^2) + a_2 S_2(\boldsymbol{v}^2) + \cdots \right), \quad \text{(B5)}$$

where the Sonine polynomials S_p are orthogonal to each other with respect to the Gaussian weight. In 2D, we notably have[60]

$$S_1(\boldsymbol{v}^2) = 1 - \boldsymbol{v}^2/v_T^2, \quad S_2(\boldsymbol{v}^2) = 1 - 2\boldsymbol{v}^2/v_T^2 + \boldsymbol{v}^4/(2v_T^4), \quad \text{(B6)}$$

with $v_T = \sqrt{2T/m}$. The temperature definition $T \equiv \frac{m}{2n} \int \boldsymbol{v}^2 f(\boldsymbol{v}) d\boldsymbol{v}$ imposes $a_1 = 0$ since $\int \boldsymbol{v}^2 f(\boldsymbol{v}^2) d\boldsymbol{v} = 2nT(1 - a_1)/m$, while the remaining non-trivial coefficients follow from the requirement that f satisfy Eq. (B1).

Multiplying Eq. (B1) by $\boldsymbol{v}^{2p}$ and integrating yields moment constraints,

$$\int \boldsymbol{v}^{2p} \mathcal{J}(\boldsymbol{v}|f,f) d\boldsymbol{v} = \frac{\sigma\chi}{2} \int \Theta(-\boldsymbol{v}_{12} \cdot \hat{\boldsymbol{\sigma}}_{12}) |\boldsymbol{v}_{12} \cdot \hat{\boldsymbol{\sigma}}_{12}| \times \left((\boldsymbol{v}_1')^{2p} + (\boldsymbol{v}_2')^{2p} - \boldsymbol{v}_1^{2p} - \boldsymbol{v}_2^{2p} \right) \times f(\boldsymbol{v}_1) f(\boldsymbol{v}_2) d\boldsymbol{v}_1 d\boldsymbol{v}_2 d\hat{\boldsymbol{\sigma}}_{12} = 0. \quad \text{(B7)}$$

Evaluating these integrals with the method presented in Appendix C 2 (see also the supplementary material) and truncating at a_2 gives, for $p = 1$,

$$(1-\alpha^2)T - m\Delta^2 + a_2 \frac{m\Delta^2 + 3(1-\alpha^2)T}{16} + \mathcal{O}(a_2^2) = 0, \quad \text{(B8)}$$

and, for $p = 2$,

$$\left(m\Delta^2 \left[m\Delta^2 + T(2\alpha^2 + 7) \right] + T^2(\alpha^2 - 1)(2\alpha^2 + 7) \right) - \frac{a_2}{16} \left(T^2(1+\alpha)\left(30\alpha^2(\alpha-1) + 177\alpha - 209\right) - m\Delta^2 \left[m\Delta^2 - T(6\alpha^2 + 29) \right] \right) + \mathcal{O}(a_2^2) = 0. \quad \text{(B9)}$$

Solving these two equations determines $T(\alpha, m\Delta^2)$ and $a_2(\alpha, m\Delta^2)$ at this order, leading to the theoretical prediction given in Fig. 5. The solution is density-independent because the sole density dependence enters through χ, which reduces to a constant prefactor in J for homogeneous states.

Other closures are possible (e.g., using $p = 1$ and $p = 3$ to get a_2 and T), but lower-order moments typically provide the most robust truncation.

APPENDIX C: CHAPMAN–ENSKOG METHODS

1. Derivation of the hydrodynamic equations

To derive the hydrodynamics equations for n, $\boldsymbol{u}$, and T [Eqs. (4)], we start from the Boltzmann–Enskog equation (14),

$$\partial_t f(\mathbf{r}, \boldsymbol{v}, t) + \boldsymbol{v} \cdot \nabla f(\mathbf{r}, \boldsymbol{v}, t) = \mathcal{J}(\mathbf{r}, \boldsymbol{v}|f,f). \quad \text{(C1)}$$

For any test function $A(\boldsymbol{v})$, multiplying by A and integrating over $\boldsymbol{v}$ gives

$$\partial_t \int A f d\boldsymbol{v} + \nabla \cdot \int A \boldsymbol{v} f d\boldsymbol{v} = \int A \mathcal{J} d\boldsymbol{v}. \quad \text{(C2)}$$

Density—With $A = 1$, mass conservation by collisions implies $\int \mathcal{J} d\boldsymbol{v} = 0$ and (C2) yields

$$\partial_t n + \nabla \cdot (n\boldsymbol{u}) = 0, \quad \text{(C3)}$$

corresponding to the continuity equation (4a).

Momentum—With $A = m\boldsymbol{v}$, Eq. (C2) gives

$$\partial_t (mn\boldsymbol{u}) + \nabla \cdot \left(m \int \boldsymbol{v} \otimes \boldsymbol{v} f d\boldsymbol{v} \right) = m \int \boldsymbol{v} \mathcal{J} d\boldsymbol{v}. \quad \text{(C4)}$$

Writing $\boldsymbol{v} = \boldsymbol{u} + \boldsymbol{c}$ and defining the kinetic stress $\boldsymbol{\Pi}^{\text{kin}} = -m \int \boldsymbol{c} \otimes \boldsymbol{c} f d\boldsymbol{v}$ and its collisional counterpart $\boldsymbol{\Pi}^{\text{coll}}$ via $\nabla \cdot \boldsymbol{\Pi}^{\text{coll}} = m \int \boldsymbol{v} \mathcal{J} d\boldsymbol{v}$, one obtains

$$\partial_t \boldsymbol{u} + \boldsymbol{u} \cdot \nabla \boldsymbol{u} = \frac{1}{mn} \nabla \cdot (\boldsymbol{\Pi}^{\text{kin}} + \boldsymbol{\Pi}^{\text{coll}}). \quad \text{(C5)}$$

The collisional stress stems from collisional momentum transfer over the contact displacement, even though each collision locally conserves $m\boldsymbol{v}$. In the dilute limit used in the main text, collisions are treated as occurring at the same point, so this contribution is neglected. We also note that $\boldsymbol{\Pi}^{\text{homo}}$ and $\boldsymbol{\Pi}^{\text{visc}}$ both get kinetic and collisional contributions.

Temperature—With $A = m\boldsymbol{c}^2/2$, Eq. (C2) yields

$$\partial_t T + \boldsymbol{u} \cdot \nabla T = \frac{1}{n} \left(\boldsymbol{\Pi} : \nabla \boldsymbol{u} - \nabla \cdot \left(\boldsymbol{J}^{\text{kin}} + \boldsymbol{J}^{\text{coll}} \right) \right) + \delta \dot{T}, \quad \text{(C6)}$$

with $\boldsymbol{J}^{\text{kin}} \equiv m \int c^2 \boldsymbol{c} f d\boldsymbol{v}/2$ and $-\nabla \cdot \boldsymbol{J}^{\text{coll}} + n\delta\dot{T} = m \int \boldsymbol{c}^2 \mathcal{J} d\boldsymbol{v}/2$. In the homogeneous state, $\boldsymbol{J} = 0$ and $\boldsymbol{u} = 0$, and Eq. (C6) reproduces Eq. (22).

2. Kinetic integrals

We repeatedly encounter matrix elements of the linearized collision operator of the form

15 July 2026 13:12:18

Published under an exclusive license by AIP Publishing

$$\left\langle \phi\left(f^{(0)}\right)^{-1}, \mathcal{L}[\psi]\right\rangle \equiv \int \phi(\boldsymbol{c}_1)\,\mathcal{L}[\psi](\boldsymbol{c}_1)d\boldsymbol{c}_1 = \chi\sigma \int \Theta(-\boldsymbol{c}_{12}\cdot\hat{\boldsymbol{\sigma}}_{12})|\boldsymbol{c}_{12}\cdot\hat{\boldsymbol{\sigma}}_{12}|\delta\phi \times \psi(\boldsymbol{c}_2)f^{(0)}(\boldsymbol{c}_1)f^{(0)}(\boldsymbol{c}_2)d\boldsymbol{c}_1 d\boldsymbol{c}_2 d\hat{\boldsymbol{\sigma}}_{12}, \quad \text{(C7)}$$

for any ϕ and ψ, and where

$$\delta\phi = \phi(\boldsymbol{c}_1') + \phi(\boldsymbol{c}_2') - \phi(\boldsymbol{c}_1) - \phi(\boldsymbol{c}_2), \quad \text{(C8)}$$

is the change of any quantity $\phi(\boldsymbol{c}_1) + \phi(\boldsymbol{c}_2)$ at collision.

These integrals simplify in center-of-mass $\boldsymbol{C} = (\boldsymbol{c}_1 + \boldsymbol{c}_2)/2$ and relative $\boldsymbol{c}_{12} = \boldsymbol{c}_1 - \boldsymbol{c}_2$. Using the collision rule (I),

$$\begin{aligned} \boldsymbol{c}_1 &= \boldsymbol{C} + \frac{1}{2}\boldsymbol{c}_{12}, \\ \boldsymbol{c}_2 &= \boldsymbol{C} - \frac{1}{2}\boldsymbol{c}_{12}, \\ \boldsymbol{c}_1' &= \boldsymbol{C} + \frac{1}{2}\boldsymbol{c}_{12} - \frac{1+\alpha}{2}(\boldsymbol{c}_{12}\cdot\hat{\boldsymbol{\sigma}}_{12})\hat{\boldsymbol{\sigma}}_{12} - \Delta\hat{\boldsymbol{\sigma}}_{12}^{\perp}, \\ \boldsymbol{c}_2' &= \boldsymbol{C} - \frac{1}{2}\boldsymbol{c}_{12} + \frac{1+\alpha}{2}(\boldsymbol{c}_{12}\cdot\hat{\boldsymbol{\sigma}}_{12})\hat{\boldsymbol{\sigma}}_{12} + \Delta\hat{\boldsymbol{\sigma}}_{12}^{\perp}. \end{aligned} \quad \text{(C9)}$$

The integrals are Gaussian and evaluated with SymPy[87] in the supplementary material by fixing

$$\boldsymbol{c}_{12} = \begin{pmatrix} s \\ 0 \end{pmatrix}, \quad \hat{\boldsymbol{\sigma}} = \begin{pmatrix} \cos(\Psi) \\ \sin(\Psi) \end{pmatrix}, \quad \boldsymbol{C} = \begin{pmatrix} C_x \\ C_y \end{pmatrix}. \quad \text{(C10)}$$

As an example, we analytically calculate the integral $\omega\langle\delta E\rangle_{\text{coll}} = \sigma\chi n^{-1}\int\Theta(-\boldsymbol{v}_{12}\cdot\hat{\boldsymbol{\sigma}}_{12})|\boldsymbol{v}_{12}\cdot\hat{\boldsymbol{\sigma}}_{12}|\delta E f(\boldsymbol{v}_2)f(\boldsymbol{v}_1)d\hat{\boldsymbol{\sigma}}_{12}d\boldsymbol{v}_1 d\boldsymbol{v}_2$, given in Eq. (22), which has the form of the previously discussed integral. We proceed by performing the change of variables in Eqs. (C9), which leads to

$$f(\boldsymbol{v}_1)f(\boldsymbol{v}_2) = \left(\frac{mn}{2\pi T}\right)^2 \exp\left(-\frac{m\boldsymbol{C}^2}{T}\right)\exp\left(-\frac{m\boldsymbol{c}_{12}^2}{4T}\right). \quad \text{(C11)}$$

Then, using the parameterization Eq. (C10) yields

$$\omega\langle\delta E\rangle_{\text{coll}} = \frac{\sigma\chi}{n}\left(\frac{mn}{2\pi T}\right)^2 \int\Theta(-\cos(\Psi))|s\cos(\Psi)|s \times \delta E e^{-m\boldsymbol{C}^2/T}e^{-ms^2/4T}d\Psi d\boldsymbol{C}ds. \quad \text{(C12)}$$

By direct computation, we obtain $\delta E = m\Delta^2 - m\Delta s\sin(\Psi) - m(1-\alpha^2)s^2\cos(\Psi)^2/4$. The term $\sin(\Psi)$ integrates to 0, while

$$\begin{aligned} \int_{\pi/2}^{3\pi/2}\cos\Psi d\Psi &= -2, \quad \int_0^{\infty} s^4 e^{-as^2}ds = \frac{3\sqrt{\pi}}{8}a^{-5/2}, \\ \int_{\pi/2}^{3\pi/2}\cos^3\Psi d\Psi &= -\frac{4}{3}, \quad \int_0^{\infty} s^2 e^{-as^2}ds = \frac{\sqrt{\pi}}{4}a^{-3/2}, \end{aligned} \quad \text{(C13)}$$

with $a = m/(4T)$. Putting everything together yields

$$\omega\langle\delta E\rangle_{\text{coll}} = 2\sqrt{\pi}\chi\sigma n\sqrt{\frac{T}{m}}\left[m\Delta^2 - (1-\alpha^2)T\right]. \quad \text{(C14)}$$

3. Viscosities

For the viscosities, we need to compute

$$\begin{aligned} \mathsf{L}_{\parallel\parallel} = \mathsf{L}_{\perp\perp} &\equiv \left\langle \left(f^{(0)}\right)^{-1} D_{ij}, \mathcal{L}[D_{ij}]\right\rangle, \\ \mathsf{L}_{\parallel\perp} = -\mathsf{L}_{\perp\parallel} &\equiv \left\langle \left(f^{(0)}\right)^{-1} D_{ij}, \mathcal{L}[D_{ij}^{\perp}]\right\rangle. \end{aligned} \quad \text{(C15)}$$

Using Eq. (C7), this gives

$$\begin{aligned} \mathsf{L}_{\parallel\parallel} &= \chi\sigma\int\Theta(-\boldsymbol{c}_{12}\cdot\hat{\boldsymbol{\sigma}})(-\boldsymbol{c}_{12}\cdot\hat{\boldsymbol{\sigma}})f^{(0)}(\boldsymbol{c}_1)f^{(0)}(\boldsymbol{c}_2) \times D_{ij}(\boldsymbol{c}_2)\delta(D_{ij})d\boldsymbol{c}_1 d\boldsymbol{c}_2 d\hat{\boldsymbol{\sigma}}, \\ \mathsf{L}_{\parallel\perp} &= \chi\sigma\int\Theta(-\boldsymbol{c}_{12}\cdot\hat{\boldsymbol{\sigma}})(-\boldsymbol{c}_{12}\cdot\hat{\boldsymbol{\sigma}})f^{(0)}(\boldsymbol{c}_1)f^{(0)}(\boldsymbol{c}_2) \times D_{ij}^{\perp}(\boldsymbol{c}_2)\delta(D_{ij})d\boldsymbol{c}_1 d\boldsymbol{c}_2 d\hat{\boldsymbol{\sigma}}. \end{aligned} \quad \text{(C16)}$$

After some algebra and using Eq. (C8), we find

$$\begin{aligned} \frac{D_{ij}(\boldsymbol{c}_2)\delta(D_{ij})}{m^2} &= (\boldsymbol{c}_1'\cdot\boldsymbol{c}_2)^2 + (\boldsymbol{c}_2'\cdot\boldsymbol{c}_2)^2 - (\boldsymbol{c}_1\cdot\boldsymbol{c}_2)^2 - (\boldsymbol{c}_2\cdot\boldsymbol{c}_2)^2 - \frac{1}{2}\boldsymbol{c}_2^2\delta(\boldsymbol{c}^2), \\ \frac{D_{ij}^{\perp}(\boldsymbol{c}_2)\delta(D_{ij})}{m^2} &= (\boldsymbol{c}_2^{\perp}\cdot\boldsymbol{c}_1')(\boldsymbol{c}_2\cdot\boldsymbol{c}_1') + (\boldsymbol{c}_2^{\perp}\cdot\boldsymbol{c}_2')(\boldsymbol{c}_2\cdot\boldsymbol{c}_2'), \end{aligned} \quad \text{(C17)}$$

with $\boldsymbol{c}^{\perp} = \boldsymbol{\varepsilon}\cdot\boldsymbol{c}$. After inserting Eq. (C9) and carrying out the Gaussian integrations, we obtain (see the supplementary material)

$$\begin{aligned} \mathsf{L}_{\parallel\parallel} &= -\chi\sigma n^2 T^2\sqrt{\frac{\pi T}{m}}\left(\frac{m\Delta^2}{T} + (1+\alpha)(7-3\alpha)\right), \\ \mathsf{L}_{\parallel\perp} &= 2\pi\chi\sigma n^2 T^2\Delta(1-\alpha). \end{aligned} \quad \text{(C18)}$$

From Eq. (53), we have

$$\begin{aligned} \eta_s &= -4n^2T^3\frac{\mathsf{L}_{\parallel\parallel}}{\mathsf{L}_{\parallel\parallel}^2 + \mathsf{L}_{\parallel\perp}^2}, \\ \eta_o &= 4n^2T^3\frac{\mathsf{L}_{\parallel\perp}}{\mathsf{L}_{\parallel\parallel}^2 + \mathsf{L}_{\parallel\perp}^2}. \end{aligned} \quad \text{(C19)}$$

After replacing $\mathsf{L}_{\parallel\parallel}$ and $\mathsf{L}_{\parallel\perp}$ by their values and replacing T by its steady-state value, we recover the main text result Eqs. (54).

We also note that the odd-viscosity

$$\eta_o = \frac{8\pi\chi\sigma n^4T^5}{\mathsf{L}_{\parallel\parallel}^2 + \mathsf{L}_{\parallel\perp}^2}\Delta(1-\alpha), \quad \text{(C20)}$$

vanishes in the limit $\alpha \to 1$, even *before* setting T to its steady-state value, as argued in the main text.

4. Thermal conductivities

Similarly to the viscosity calculation, the thermal sector requires the matrix elements,

$$\mathsf{M}_{\alpha\beta} \equiv \left\langle \left(f^{(0)}\right)^{-1} A_i^{(\alpha)}, \mathcal{L}[A_i^{(\beta)}]\right\rangle, \quad \alpha,\beta \in \{\parallel,\perp\}, \quad \text{(C21)}$$

15 July 2026 13:12:18

Published under an exclusive license by AIP Publishing

with $A_i^{(\parallel)} \equiv A_i$ and $A_i^{(\perp)} \equiv A_i^\perp$. Projecting the thermal part of Eq. (42) onto $\{\mathbf{A}, \mathbf{A}^\perp\}$ gives

$$\frac{1}{T}\begin{pmatrix} 4nT^3/m \\ 0 \end{pmatrix} = \begin{pmatrix} \mathsf{M}_{\parallel\parallel} & \mathsf{M}_{\parallel\perp} \\ \mathsf{M}_{\perp\parallel} & \mathsf{M}_{\perp\perp} \end{pmatrix}\begin{pmatrix} \mathcal{A}_0 \\ \mathcal{A}_0^\perp \end{pmatrix}, \tag{C22}$$

where we used $\langle A_i, A_j\rangle = (2nT^3/m)\delta_{ij}$ and $\langle A_i^\perp, A_i\rangle = 0$. The inversion yields

$$\mathcal{A}_0 = \frac{4nT^2}{m}\frac{\mathsf{M}_{\parallel\parallel}}{\mathsf{M}_{\parallel\parallel}^2 + \mathsf{M}_{\parallel\perp}^2}, \quad \mathcal{A}_0^\perp = \frac{4nT^2}{m}\frac{\mathsf{M}_{\parallel\perp}}{\mathsf{M}_{\parallel\parallel}^2 + \mathsf{M}_{\parallel\perp}^2}. \tag{C23}$$

The matrix elements follow from the kinetic integral (C7) with integrands,

$$\begin{aligned} \frac{A_i(\boldsymbol{c}_2)\delta(A_i)}{m/2} &= \left(\frac{m\boldsymbol{c}_2^2}{2} - 2T\right)\left[\boldsymbol{c}_1'^2(\boldsymbol{c}_2\cdot\boldsymbol{c}_1') + \boldsymbol{c}_2'^2(\boldsymbol{c}_2\cdot\boldsymbol{c}_2')\right. \\ &\quad \left. - \boldsymbol{c}_1^2(\boldsymbol{c}_2\cdot\boldsymbol{c}_1) - \boldsymbol{c}_2^2(\boldsymbol{c}_2\cdot\boldsymbol{c}_2)\right], \\ \frac{A_i^\perp(\boldsymbol{c}_2)\delta(A_i)}{m/2} &= \left(\frac{m\boldsymbol{c}_2^2}{2} - 2T\right)\left[\boldsymbol{c}_1'^2(\boldsymbol{c}_2^\perp\cdot\boldsymbol{c}_1') + \boldsymbol{c}_2'^2(\boldsymbol{c}_2^\perp\cdot\boldsymbol{c}_2')\right. \\ &\quad \left. - \boldsymbol{c}_1^2(\boldsymbol{c}_2^\perp\cdot\boldsymbol{c}_1) - \boldsymbol{c}_2^2(\boldsymbol{c}_2^\perp\cdot\boldsymbol{c}_2)\right]. \end{aligned} \tag{C24}$$

Upon integration, we obtain (see the supplementary material)

$$\begin{aligned} \mathsf{M}_{\parallel\parallel} &= -\frac{\sqrt{\pi}T^{5/2}\chi n^2\sigma}{2m^{3/2}}\left(T(1+\alpha)(19-15\alpha) - 3m\Delta^2\right), \\ \mathsf{M}_{\parallel\perp} &= \pi\chi\sigma n^2 T^3\Delta(1-\alpha)/m. \end{aligned} \tag{C25}$$

To relate M to the conductivities, we use the heat current

$$\begin{aligned} \boldsymbol{J} &= \frac{m}{2}\int \boldsymbol{c}^2\boldsymbol{c}f(\boldsymbol{c})d\boldsymbol{c} \\ &= \mu\frac{m}{2T}\int \boldsymbol{c}^2\boldsymbol{c}f^{(0)}(\boldsymbol{c})\left(\mathcal{A}_0\mathbf{A} + \mathcal{A}_0^\perp\mathbf{A}^\perp\right)\cdot\nabla T d\boldsymbol{c} \\ &= \mu\left(\frac{2nT^2}{m}\mathcal{A}_0\mathbf{1} - \frac{2nT^2}{m}\mathcal{A}_0^\perp\boldsymbol{\varepsilon}\right)\nabla T, \end{aligned} \tag{C26}$$

so that

$$\kappa = -\frac{2nT^2}{m}\mathcal{A}_0, \qquad \kappa_o = \frac{2nT^2}{m}\mathcal{A}_0^\perp. \tag{C27}$$

Substituting Eq. (C23) and the steady-state temperature yields

$$\kappa = \frac{16|\Delta|(1+\alpha)(4-3\alpha)}{\sqrt{\pi}\chi\sigma\sqrt{1-\alpha^2}Q(\alpha)}, \tag{C28}$$

$$\kappa_o = \frac{8\Delta(1-\alpha)}{\chi\sigma Q(\alpha)}, \tag{C29}$$

with $Q(\alpha)$ a positive polynomial over $0 \le \alpha \le 1$,

$$Q(\alpha) = \pi(1-\alpha)^2(1-\alpha^2) + 4(1+\alpha)^2(4-3\alpha)^2. \tag{C30}$$

5. Self-diffusion coefficient

We compute the regular self-diffusivity D and its odd counterpart D_o from the Boltzmann–Lorentz equation for a tracer following Ref. 60,

$$\partial_t f_s(\mathbf{r},\boldsymbol{v},t) + \boldsymbol{v}\cdot\nabla f_s(\mathbf{r},\boldsymbol{v},t) = \mathcal{J}^{\text{dilute}}(\mathbf{r},\boldsymbol{v}|f_s,f_B), \tag{C31}$$

where $f_B = f^{(0)}$ is a fixed *homogeneous* Gaussian and only f_s evolves with time. The tracer density $n_s(\mathbf{r},t) = \int f_s(\mathbf{r},\boldsymbol{v},t)d\boldsymbol{v}$ obeys

$$\partial_t n_s = -\nabla\cdot\boldsymbol{J}_s, \quad \boldsymbol{J}_s = -D\nabla n_s - D_o(\boldsymbol{\varepsilon}\cdot\nabla)n_s. \tag{C32}$$

We use a Chapman–Enskog expansion with, for convenience, a slightly modified ansatz relative to the main text

$$f_s(\mathbf{r},\boldsymbol{v},t) = f_s^{(0)}[n_s(\mathbf{r},t)|\boldsymbol{v}] + \mu f_s^{(1)}[n_s(\mathbf{r},t)|\boldsymbol{v}]. \tag{C33}$$

Since tracer and bath particles are identical, their homogeneous distribution must be the same,

$$f_s^{(0)} = \frac{n_s(\mathbf{r},t)}{n}f_B, \tag{C34}$$

where $n = (N-1)/L^2 \simeq N/L^2$ is the global bath number density. At order μ^1, the Boltzmann–Lorentz equation reads

$$\partial_t^{(0)} f_s^{(1)} + \partial_t^{(1)} f_s^{(0)} + \boldsymbol{v}\cdot\nabla f_s^{(0)} = \mathcal{J}^{\text{dilute}}(f_B, f_s^{(1)}). \tag{C35}$$

In the steady state $\partial_t^{(0)} f_s^{(1)} = 0$, and since $\partial_t n_s = \mathcal{O}(\nabla^2)$ we also have $\partial_t^{(1)} f_s^{(0)} = 0$, yielding

$$\frac{1}{n}(\boldsymbol{v}\cdot\nabla n_s)f_B = \mathcal{J}^{\text{dilute}}(f_B, f_s^{(1)}). \tag{C36}$$

By linearity of $\mathcal{J}^{\text{dilute}}(f_B,\cdots)$, we seek a solution of the form

$$f_s^{(1)} = (B(\boldsymbol{v})\boldsymbol{v}\cdot\nabla n_s + B^\perp(\boldsymbol{v})\boldsymbol{v}^\perp\cdot\nabla n_s)f_B(\boldsymbol{v}), \tag{C37}$$

with $\boldsymbol{v}^\perp = \boldsymbol{\varepsilon}\cdot\boldsymbol{v}$. We assume again $B(\boldsymbol{v}) = B_0$ and $B^\perp(\boldsymbol{v}) = B_0^\perp$. Therefore, we must solve

$$\frac{1}{n}f_B\boldsymbol{v} = B_0\mathcal{J}^{\text{dilute}}(f_B, f_B\boldsymbol{v}) + B_0^\perp\mathcal{J}^{\text{dilute}}(f_B, f_B\boldsymbol{v}^\perp). \tag{C38}$$

Projecting onto $\{\boldsymbol{v},\boldsymbol{v}^\perp\}$ yields

$$\frac{1}{n}\begin{pmatrix} 2nT/m \\ 0 \end{pmatrix} = \begin{pmatrix} \mathsf{N}_{\parallel\parallel} & \mathsf{N}_{\parallel\perp} \\ -\mathsf{N}_{\parallel\perp} & \mathsf{N}_{\parallel\parallel} \end{pmatrix}\begin{pmatrix} B_0 \\ B_0^\perp \end{pmatrix}, \tag{C39}$$

with (see the supplementary material)

$$\begin{aligned} \mathsf{N}_{\parallel\parallel} &= \int \boldsymbol{v}\cdot\mathcal{J}^{\text{dilute}}(f_B, f_B\boldsymbol{v})d\boldsymbol{v} \\ &= -2\sqrt{\pi(T/m)^3}\chi n^2\sigma(1+\alpha), \\ \mathsf{N}_{\parallel\perp} &= \int \boldsymbol{v}\cdot\mathcal{J}^{\text{dilute}}(f_B, f_B\boldsymbol{v}^\perp)d\boldsymbol{v} \\ &= \frac{\pi\sigma\chi n^2 T}{m}\Delta. \end{aligned} \tag{C40}$$

15 July 2026 13:12:18

Published under an exclusive license by AIP Publishing

We now relate B_0 and $B_0^\perp$ to the diffusivities via $\boldsymbol{J}_s = \int \boldsymbol{v} f_s d\boldsymbol{v}$,

$$\begin{aligned}\boldsymbol{J}_s &= \mu \int \boldsymbol{v} f_B(\boldsymbol{v}) \left(B_0 \boldsymbol{v} + B_0^\perp \boldsymbol{v}^\perp\right) \cdot \nabla n_s d\boldsymbol{v} \\ &= \mu \frac{nT}{m} \left(B_0 \boldsymbol{1} - B_0^\perp \boldsymbol{\varepsilon}\right) \cdot \nabla n_s. \end{aligned} \tag{C41}$$

By identifying with Eq. (C32), we obtain

$$D = -\frac{nT}{m} B_0, \quad D_o = \frac{nT}{m} B_0^\perp. \tag{C42}$$

Inverting Eq. (C39) and using the steady state temperature Eq. (24) yields

$$D = \frac{\sqrt{\pi}\sigma|\Delta|}{\phi\chi\sqrt{1-\alpha^2}R(\alpha)}, \quad D_o = \frac{\pi\sigma\Delta}{2\phi\chi(1+\alpha)R(\alpha)}, \tag{C43}$$

with $R(\alpha)$ a strictly positive polynomial over $0 \le \alpha \le 1$,

$$R(\alpha) = 4(1+\alpha) + \pi(1-\alpha). \tag{C44}$$

REFERENCES

[1] H. Löwen, "Chirality in microswimmer motion: From circle swimmers to active turbulence," Eur. Phys. J.: Spec. Top. **225**, 2319–2331 (2016).
[2] B. Liebchen and D. Levis, "Chiral active matter," Europhys. Lett. **139**, 67001 (2022).
[3] D. M. Woolley, "Motility of spermatozoa at surfaces," Reproduction **126**, 259 (2003).
[4] A. P. Petroff, X.-L. Wu, and A. Libchaber, "Fast-moving bacteria self-organize into active two-dimensional crystals of rotating cells," Phys. Rev. Lett. **114**, 158102 (2015).
[5] J. Xu, A. Van Keymeulen, N. M. Wakida, P. Carlton, M. W. Berns, and H. R. Bourne, "Polarity reveals intrinsic cell chirality," Proc. Natl. Acad. Sci. U. S. A. **104**, 9296 (2007).
[6] M. Huang, W. Hu, S. Yang, Q.-X. Liu, and H. P. Zhang, "Circular swimming motility and disordered hyperuniform state in an algae system," Proc. Natl. Acad. Sci. U. S. A. **118**, e2100493118 (2021).
[7] T. H. Tan, A. Mietke, J. Li, Y. Chen, H. Higinbotham, P. J. Foster, S. Gokhale, J. Dunkel, and N. Fakhri, "Odd dynamics of living chiral crystals," Nature **607**, 287–293 (2022).
[8] F. Kümmel, B. Ten Hagen, R. Wittkowski, I. Buttinoni, R. Eichhorn, G. Volpe, H. Löwen, and C. Bechinger, "Circular motion of asymmetric self-propelling particles," Phys. Rev. Lett. **110**, 198302 (2013).
[9] F. Siebers, A. Jayaram, P. Blümler, and T. Speck, "Exploiting compositional disorder in collectives of light-driven circle walkers," Sci. Adv. **9**, eadf5443 (2023).
[10] J. P. Carrillo-Mora, A. Garcés, and D. Levis, "Depinning and activated motion of chiral self-propelled particles," Phys. Rev. E **112**, 065417 (2025).
[11] C. Scholz, M. Engel, and T. Pöschel, "Rotating robots move collectively and self-organize," Nat. Commun. **9**, 931 (2018).
[12] L. Caprini, I. Abdoli, U. Marini Bettolo Marconi, and H. Löwen, "Spontaneous self-wrapping in chiral active polymers," Newton **1**, 100253 (2025).
[13] U. Tiwari, P. Arora, A. Sood, S. Ramaswamy, R. Mandal, and R. Ganapathy, "Reentrant melting of scarred odd crystals by self-shear," Nat. Commun. **17**, 1802 (2026).
[14] R. Huang, R. Mandal, C. Scheibner, and V. Vitelli, "Odd elasticity in driven granular matter," arXiv:2311.18720 (2023).
[15] M. A. López-Castaño, A. M. Seco, A. M. Seco, Á. Rodríguez-Rivas, and F. V. Reyes, "Chirality transitions in a system of active flat spinners," Phys. Rev. Res. **4**, 033230 (2022).
[16] F. Vega Reyes, M. A. López-Castaño, and Á. Rodríguez-Rivas, "Diffusive regimes in a two-dimensional chiral fluid," Commun. Phys. **5**, 256 (2022).
[17] L. Caprini and U. Marini Bettolo Marconi, "Active chiral particles under confinement: Surface currents and bulk accumulation phenomena," Soft Matter **15**, 2627–2637 (2019).
[18] D. Levis, I. Pagonabarraga, and B. Liebchen, "Activity induced synchronization: Mutual flocking and chiral self-sorting," Phys. Rev. Res. **1**, 023026 (2019).
[19] K. L. Kreienkamp and S. H. L. Klapp, "Clustering and flocking of repulsive chiral active particles with non-reciprocal couplings," New J. Phys. **24**, 123009 (2022).
[20] J. Bickmann, S. Bröker, J. Jeggle, and R. Wittkowski, "Analytical approach to chiral active systems: Suppressed phase separation of interacting Brownian circle swimmers," J. Chem. Phys. **156**, 194904 (2022).
[21] G. Pisegna and S. Saha, "Spinning mixtures: Nonreciprocity transfers chirality across scales in scalar densities," arXiv:2509.07630 (2025).
[22] M. Workamp, G. Ramirez, K. E. Daniels, and J. A. Dijksman, "Symmetry-reversals in chiral active matter," Soft Matter **14**, 5572–5580 (2018).
[23] J. Mecke, J. O. Nketsiah, R. Li, and Y. Gao, "Emergent phenomena in chiral active matter," Natl. Sci. Open **3**, 20230086 (2024).
[24] A. Negi, K. Beppu, and Y. T. Maeda, "Geometry-induced dynamics of confined chiral active matter," Phys. Rev. Res. **5**, 023196 (2023).
[25] L. Caprini, U. M. B. Marconi, B. Liebchen, and H. Löwen, "Active thermodynamics of inertial chiral active gases: Equation of state and edge currents," arXiv:2509.05053 (2025).
[26] L. Caprini, H. Löwen, and U. Marini Bettolo Marconi, "Chiral active matter in external potentials," Soft Matter **19**, 6234–6246 (2023).
[27] Z.-F. Huang, A. M. Menzel, and H. Löwen, "Dynamical crystallites of active chiral particles," Phys. Rev. Lett. **125**, 218002 (2020).
[28] M. Musacchio, A. P. Antonov, H. Löwen, and L. Caprini, "Circling crystals in chiral active matter with self-alignment," Soft Matter **22**, 2052 (2026).
[29] C. Hargus, J. M. Epstein, and K. K. Mandadapu, "Odd diffusivity of chiral random motion," Phys. Rev. Lett. **127**, 178001 (2021).
[30] I. Abdoli, R. Wittmann, and H. Löwen, "Dynamical density functional theory for dense odd-diffusive fluids," J. Phys. Chem. B. **130**(17), 4672–4682 (2026).
[31] F. Faedi, E. Kalz, R. Metzler, and A. Sharma, "A mobility based approach to transport in chiral fluids," New J. Phys. **28**(6), 063501 (2026).
[32] C. Reichhardt and C. J. O. Reichhardt, "Active microrheology, Hall effect, and jamming in chiral fluids," Phys. Rev. E **100**, 012604 (2019).
[33] C. J. O. Reichhardt and C. Reichhardt, "Active rheology in odd-viscosity systems," Europhys. Lett. **137**, 66004 (2022).
[34] E. Kalz, H. D. Vuijk, I. Abdoli, J.-U. Sommer, H. Löwen, and A. Sharma, "Collisions enhance self-diffusion in odd-diffusive systems," Phys. Rev. Lett. **129**, 090601 (2022).
[35] E. Kalz, H. D. Vuijk, J.-U. Sommer, R. Metzler, and A. Sharma, "Oscillatory force autocorrelations in equilibrium odd-diffusive systems," Phys. Rev. Lett. **132**, 057102 (2024).
[36] K. Everschor-Sitte and M. Sitte, "Real-space Berry phases: Skyrmion soccer," J. Appl. Phys. **115**, 172602 (2014).
[37] M. Weißenhofer, L. Rózsa, and U. Nowak, "Skyrmion dynamics at finite temperatures: Beyond Thiele's equation," Phys. Rev. Lett. **127**, 047203 (2021).
[38] T. Dohi, M. Weißenhofer, N. Kerber, F. Kammerbauer, Y. Ge, K. Raab, J. Zázvorka, M.-A. Syskaki, A. Shahee, M. Ruhwedel *et al.*, "Enhanced thermally-activated skyrmion diffusion with tunable effective gyrotropic force," Nat. Commun. **14**, 5424 (2023).
[39] M. Fruchart, C. Scheibner, and V. Vitelli, "Odd viscosity and odd elasticity," Annu. Rev. Condens. Matter Phys. **14**, 471–510 (2023).
[40] D. Banerjee, A. Souslov, A. G. Abanov, and V. Vitelli, "Odd viscosity in chiral active fluids," Nat. Commun. **8**, 1573 (2017).
[41] T. Markovich and T. C. Lubensky, "Odd viscosity in active matter: Microscopic origin and 3D effects," Phys. Rev. Lett. **127**, 048001 (2021).
[42] T. Markovich and T. C. Lubensky, "Chiral active fluids: Insights from the total momentum," Phys. Rev. E **112**, 035409 (2025).
[43] J. E. Avron, "Odd viscosity," J. Stat. Phys. **92**, 543–557 (1998).
[44] V. Soni, E. S. Bililign, S. Magkiriadou, S. Sacanna, D. Bartolo, M. J. Shelley, and W. T. M. Irvine, "The odd free surface flows of a colloidal chiral fluid," Nat. Phys. **15**, 1188–1194 (2019).
[45] A. I. Berdyugin, S. G. Xu, F. M. D. Pellegrino, R. Krishna Kumar, A. Principi, I. Torre, M. Ben Shalom, T. Taniguchi, K. Watanabe, I. V. Grigorieva *et al.*,

15 July 2026 13:12:18

Published under an exclusive license by AIP Publishing

"Measuring Hall viscosity of graphene's electron fluid," Science **364**, 162–165 (2019).
[46]X. Lou, Q. Yang, Y. Ding, P. Liu, K. Chen, X. Zhou, F. Ye, R. Podgornik, and M. Yang, "Odd viscosity-induced Hall-like transport of an active chiral fluid," Proc. Natl. Acad. Sci. U. S. A. **119**, e2201279119 (2022).
[47]R. Lier, C. Duclut, S. Bo, J. Armas, F. Jülicher, and P. Surówka, "Lift force in odd compressible fluids," Phys. Rev. E **108**, L023101 (2023).
[48]Y. Hosaka, R. Golestanian, and A. Vilfan, "Lorentz reciprocal theorem in fluids with odd viscosity," Phys. Rev. Lett. **131**, 178303 (2023).
[49]Z.-F. Huang, M. te Vrugt, R. Wittkowski, and H. Löwen, "Anomalous grain dynamics and grain locomotion of odd crystals," Proc. Natl. Acad. Sci. U. S. A. **122**, e2511350122 (2025).
[50]U. Marini Bettolo Marconi, A. Petrini, R. Maire, and L. Caprini, "Emergent hydrodynamics of chiral active fluids: vortices, bubbles and odd diffusion," New J. Phys. **28**(6), 064401 (2026).
[51]L. Caprini and U. Marini Bettolo Marconi, "Bubble phase induced by odd interactions in chiral systems," J. Chem. Phys. **162**, 161101 (2025).
[52]C. B. Caporusso, G. Gonnella, and D. Levis, "Phase coexistence and edge currents in the chiral Lennard–Jones fluid," Phys. Rev. Lett. **132**, 168201 (2024).
[53]L. Caprini, A. Petrini, and U. Marini Bettolo Marconi, "Modeling chiral active particles: From circular motion to odd interactions," J. Stat. Mech.: Theory Exp. **2026**(2), 024001.
[54]P. Digregorio, I. Pagonabarraga, and F. Vega Reyes, "Phase separation in a chiral active fluid of inertial self-spinning disks," Phys. Rev. Lett. **136**(21), 218301 (2026).
[55]R.-x. Guo, M.-z. Dai, J.-j. Li, and B.-q. Ai, "Tuning nonequilibrium phases with odd forces: From crystalline order to vortex structures in systems with competing interactions," Phys. Rev. E **113**, 024110 (2026).
[56]C.-T. Lee, T. C. Lubensky, and T. Markovich, "Odd elasticity in disordered chiral active materials," arXiv:2508.04468 (2025).
[57]L. Braverman, C. Scheibner, B. VanSaders, and V. Vitelli, "Topological defects in solids with odd elasticity," Phys. Rev. Lett. **127**, 268001 (2021).
[58]E. Eren, M. Fruchart, and V. Vitelli, "A collisional model of odd fluids: From Boltzmann equation to chiral hydrodynamics," arXiv:2508.12944 (2025).
[59]R. Lier and P. Matus, "Chapman–Enskog expansion for chirally colliding disks," arXiv:2602.21367 (2026).
[60]N. V. Brilliantov and T. Pöschel, *Kinetic Theory of Granular Gases* (Oxford University Press, 2010).
[61]R. Maire and L. Chaix, "Hyperuniformity and conservation laws in non-equilibrium systems," J. Chem. Phys. **163**, 214507 (2025).
[62]H. Massana-Cid, D. Levis, R. J. H. Hernández, I. Pagonabarraga, and P. Tierno, "Arrested phase separation in chiral fluids of colloidal spinners," Phys. Rev. Res. **3**, L042021 (2021).
[63]J. Mecke, Y. Gao, C. A. Ramírez Medina, D. G. A. L. Aarts, G. Gompper, and M. Ripoll, "Simultaneous emergence of active turbulence and odd viscosity in a colloidal chiral active system," Commun. Phys. **6**, 324 (2023).
[64]T. C. Lubensky, "Phenomenological dynamics: From Navier–Stokes to chiral granular gases," Pramana **64**, 727–742 (2005).
[65]J.-C. Tsai, F. Ye, J. Rodriguez, J. P. Gollub, and T. C. Lubensky, "A chiral granular gas," Phys. Rev. Lett. **94**, 214301 (2005).
[66]M. Han, M. Fruchart, C. Scheibner, S. Vaikuntanathan, J. J. De Pablo, and V. Vitelli, "Fluctuating hydrodynamics of chiral active fluids," Nat. Phys. **17**, 1260–1269 (2021).
[67]N. H. Nguyen, D. Klotsa, M. Engel, and S. C. Glotzer, "Emergent collective phenomena in a mixture of hard shapes through active rotation," Phys. Rev. Lett. **112**, 075701 (2014).
[68]B. C. Van Zuiden, J. Paulose, W. T. M. Irvine, D. Bartolo, and V. Vitelli, "Spatiotemporal order and emergent edge currents in active spinner materials," Proc. Natl. Acad. Sci. U. S. A. **113**, 12919–12924 (2016).
[69]K. Yeo, E. Lushi, and P. M. Vlahovska, "Collective dynamics in a binary mixture of hydrodynamically coupled microrotors," Phys. Rev. Lett. **114**, 188301 (2015).
[70]S. Fürthauer, M. Strempel, S. W. Grill, and F. Jülicher, "Active chiral fluids," Eur. Phys. J. E **35**, 89 (2012).
[71]S. Gao, H. Shang, H. Hu, Y.-Q. Ma, and Q.-L. Lei, "Liquid-gas criticality of hyperuniform fluids," Phys. Rev. X **16**, 021032 (2025).
[72]S. Van Teeffelen and H. Löwen, "Dynamics of a Brownian circle swimmer," Phys. Rev. E **78**, 020101 (2008).
[73]F. J. Sevilla, "Diffusion of active chiral particles," Phys. Rev. E **94**, 062120 (2016).
[74]Y. Kuroda and K. Miyazaki, "Microscopic theory for hyperuniformity in two-dimensional chiral active fluid," J. Stat. Mech.: Theory Exp. **2023**, 103203.
[75]Y. Kuroda, T. Kawasaki, and K. Miyazaki, "Singular density correlations in chiral active fluids in three dimensions," Phys. Rev. E **112**, 045426 (2025).
[76]L. Caprini, B. Liebchen, and H. Löwen, "Self-reverting vortices in chiral active matter," Commun. Phys. **7**, 153 (2024).
[77]Q.-L. Lei, M. P. Ciamarra, and R. Ni, "Nonequilibrium strongly hyperuniform fluids of circle active particles with large local density fluctuations," Sci. Adv. **5**, eaau7423 (2019).
[78]F. Smallenburg, "Efficient event-driven simulations of hard spheres," Eur. Phys. J. E **45**, 22 (2022).
[79]J.-P. Hansen and I. R. McDonald, *Theory of Simple Liquids: With Applications to Soft Matter* (Academic Press, 2013).
[80]J. W. Dufty and J. J. Brey, "Choosing hydrodynamic fields," Math. Modell. Nat. Phenom. **6**, 19–36 (2011).
[81]P. M. Chaikin, T. C. Lubensky, and T. A. Witten, *Principles of Condensed Matter Physics* (Cambridge University Press Cambridge, 1995), Vol. 10.
[82]A. Mulero, I. Cachadiña, and J. R. Solana, "The equation of state of the hard-disc fluid revisited," Mol. Phys. **107**, 1457–1465 (2009).
[83]Z. Shen and J. S. Lintuvuori, "Collective flows drive cavitation in spinner monolayers," Phys. Rev. Lett. **130**, 188202 (2023).
[84]R.-x. Guo, J.-j. Li, and B.-q. Ai, "Chirality-induced phase separation and collective dynamics in binary mixtures of chiral particles," Phys. Rev. E **111**, 045423 (2025).
[85]M. F. Lapa and T. L. Hughes, "Swimming at low Reynolds number in fluids with odd, or hall, viscosity," Phys. Rev. E **89**, 043019 (2014).
[86]M. Fruchart, M. Han, C. Scheibner, and V. Vitelli, "The odd ideal gas: Hall viscosity and thermal conductivity from non-Hermitian kinetic theory," arXiv:2202.02037 (2022).
[87]A. Meurer, C. P. Smith, M. Paprocki, O. Čertík, S. B. Kirpichev, M. Rocklin, A. Kumar, S. Ivanov, J. K. Moore, S. Singh, T. Rathnayake, S. Vig, B. E. Granger, R. P. Muller, F. Bonazzi, H. Gupta, S. Vats, F. Johansson, F. Pedregosa, M. J. Curry, A. R. Terrel, Š. Roučka, A. Saboo, I. Fernando, S. Kulal, R. Cimrman, and A. Scopatz, "SymPy: Symbolic computing in Python," PeerJ Comput. Sci. **3**, e103 (2017).
[88]S. Chapman and T. Cowling, *The Mathematical Theory of Non-Uniform Gases: An Account of the Kinetic Theory of Viscosity, Thermal Conduction and Diffusion in Gases*, *Cambridge Mathematical Library* (Cambridge University Press, 1990).
[89]I. Pagonabarraga, E. Trizac, T. P. C. van Noije, and M. H. Ernst, "Randomly driven granular fluids: Collisional statistics and short scale structure," Phys. Rev. E **65**, 011303 (2001).
[90]R. Soto, J. Piasecki, and M. Mareschal, "Precollisional velocity correlations in a hard-disk fluid with dissipative collisions," Phys. Rev. E **64**, 031306 (2001).
[91]T. P. C. van Noije, M. H. Ernst, and R. Brito, "Ring kinetic theory for an idealized granular gas," Physica A **251**, 266–283 (1998).
[92]R. Maire, A. Plati, M. Stockinger, E. Trizac, F. Smallenburg, and G. Foffi, "Interplay between an absorbing phase transition and synchronization in a driven granular system," Phys. Rev. Lett. **132**, 238202 (2024).
[93]R. Brito, D. Risso, and R. Soto, "Hydrodynamic modes in a confined granular fluid," Phys. Rev. E **87**, 022209 (2013).
[94]R. Maire, A. Plati, F. Smallenburg, and G. Foffi, "Non-equilibrium coexistence between a fluid and a hotter or colder crystal of granular hard disks," J. Chem. Phys. **162**, 124901 (2025).
[95]R. Soto and M. Mareschal, "Statistical mechanics of fluidized granular media: Short-range velocity correlations," Phys. Rev. E **63**, 041303 (2001).
[96]J. R. Dorfman, H. van Beijeren, and T. R. Kirkpatrick, *Contemporary Kinetic Theory of Matter* (Cambridge University Press, 2021).
[97]T. Ihle, "Kinetic theory of flocking: Derivation of hydrodynamic equations," Phys. Rev. E **83**, 030901 (2011).
[98]G. Gonnella, D. Marenduzzo, A. Suma, and A. Tiribocchi, "Motility-induced phase separation and coarsening in active matter," C. R. Phys. **16**, 316–331 (2015).

15 July 2026 13:12:18

Published under an exclusive license by AIP Publishing

[99]P. Degond and T. Yang, "Diffusion in a continuum model of self-propelled particles with alignment interaction," Math. Models Methods Appl. Sci. **20**, 1459–1490 (2010).
[100]B. Hancock and A. Baskaran, "Statistical mechanics and hydrodynamics of self-propelled hard spheres," J. Stat. Mech.: Theory Exp. **2017**, 033205.
[101]A. B. T. Barbaro and P. Degond, "Phase transition and diffusion among socially interacting self-propelled agents," Discrete Contin. Dyn. Syst. - B **19**, 1249–1278 (2014).
[102]L. L. Bonilla, "Active Ornstein–Uhlenbeck particles," Phys. Rev. E **100**, 022601 (2019).
[103]D. Marenduzzo, "An introduction to the statistical physics of active matter: Motility-induced phase separation and the 'generic instability' of active gels," Eur. Phys. J.: Spec. Top. **225**, 2065–2077 (2016).
[104]M. Pinto-Goldberg and R. Soto, "Hydrodynamic equations for active Brownian particles in the high-persistence regime," Phys. Rev. E **112**, 065413 (2025).
[105]O. Feliachi, M. Besse, C. Nardini, and J. Barré, "Fluctuating kinetic theory and fluctuating hydrodynamics of aligning active particles: The dilute limit," J. Stat. Mech.: Theory Exp. **2022**, 113207.
[106]D. Nesbitt, G. Pruessner, and C. F. Lee, "Uncovering novel phase transitions in dense dry polar active fluids using a lattice Boltzmann method," New J. Phys. **23**, 043047 (2021).
[107]J. J. Brey, V. Buzón, P. Maynar, and M. I. García de Soria, "Hydrodynamics for a model of a confined quasi-two-dimensional granular gas," Phys. Rev. E **91**, 052201 (2015).
[108]P. Rosenau, "Extending hydrodynamics via the regularization of the Chapman–Enskog expansion," Phys. Rev. A **40**, 7193 (1989).
[109]A. V. Bobylev, "Instabilities in the Chapman–Enskog expansion and hyperbolic Burnett equations," J. Stat. Phys. **124**, 371–399 (2006).
[110]V. Garzó, R. Brito, and R. Soto, "Enskog kinetic theory for a model of a confined quasi-two-dimensional granular fluid," Phys. Rev. E **98**, 052904 (2018).
[111]D. G. Méndez and V. Garzó, "Transport properties in a model of confined granular mixtures at moderate densities," Phys. Fluids **38**(3), 033343 (2026).
[112]H. Nakano, Y. Minami, and K. Saito, "Looking at bare transport coefficients in fluctuating hydrodynamics," arXiv:2502.15241 (2025).
[113]Y. Pomeau and P. Résibois, "Time dependent correlation functions and mode-mode coupling theories," Phys. Rep. **19**, 63–139 (1975).
[114]This choice is not merely conventional: In the Chapman–Enskog expansion, one *identifies* the hydrodynamic fields with the corresponding velocity moments of $f^{(0)}$. As a result, the higher-order corrections do not contribute to those moments: $\int f^{(0)}(\boldsymbol{v})\Phi^{(1)}(\boldsymbol{v})\Psi(\boldsymbol{v})d\boldsymbol{v} = 0$ with $\Psi \in \{1, \boldsymbol{v}, \boldsymbol{v}^2\}$. These moment constraints are known as the solvability (Fredholm) conditions for the linear equation $\mathcal{L}[\Phi^{(1)}] = S$ (defined below), which impose the source term S to be orthogonal to $\ker(\mathcal{L}^\dagger)$, which is spanned by the collision invariants ($\boldsymbol{v}^2$ is also included in our energy-nonconserving system to recover the proper nonchiral limit). Since $\mathcal{L}$ has a nontrivial null space, it is not invertible on the full function space. Enforcing the above orthogonality removes the null modes and guarantees the existence of $\Phi^{(1)}$.
[115]C. Bardos, F. Golse, and D. Levermore, "Fluid dynamic limits of kinetic equations. I. Formal derivations," J. Stat. Phys. **63**, 323–344 (1991).
[116]F. Golse, "The Boltzmann equation and its hydrodynamic limits," in *Handbook of Differential Equations: Evolutionary Equations* (Elsevier, 2005), Vol. 2, pp. 159–301.
[117]G. M. Kremer, A. Santos, and V. Garzó, "Transport coefficients of a granular gas of inelastic rough hard spheres," Phys. Rev. E **90**, 022205 (2014).
[118]P. Résibois, "On linearized hydrodynamic modes in statistical physics," J. Stat. Phys. **2**, 21–51 (1970).
[119]R. Soto, D. Risso, and R. Brito, "Shear viscosity of a model for confined granular media," Phys. Rev. E **90**, 062204 (2014).
[120]R. Gómez González, V. Garzó, R. Brito, and R. Soto, "Diffusion of impurities in a moderately dense confined granular gas," Phys. Fluids **36**, 123387 (2024).
[121]R.-x. Guo, J.-j. Li, and B.-q. Ai, "Diffusion of active particles driven by odd interactions," Phys. Rev. E **111**, 014105 (2025).
[122]P. Luigi Muzzeddu, E. Kalz, A. Gambassi, A. Sharma, and R. Metzler, "Self-diffusion anomalies of an odd tracer in soft-core media," New J. Phys. **27**, 033025 (2025).
[123]V. Garzó and J. M. Montanero, "Transport coefficients of a heated granular gas," Physica A **313**, 336–356 (2002).
[124]W. Shi, D. T. Lam Nguyen, W. J. Goh, H. T. Ong, R. Bin Tan, C. Fu, A. D. Bershadsky, A. Mogilner, and Y. H. Tee, "Ordering from the edge: Chiral multicellular pattern formation directed by actin self-organisation in cells," bioRxiv:2025.10.14.682394 (2025).
[125]J. Chen, X. Lei, Y. Xiang, M. Duan, X. Peng, and H. Zhang, "Emergent chirality and hyperuniformity in an active mixture with nonreciprocal interactions," Phys. Rev. Lett. **132**, 118301 (2024).
[126]H. Li, H. Chaté, M. Sano, X.-q. Shi, and H. Zhang, "Robust edge flows in swarming bacterial colonies," Phys. Rev. X **14**, 041006 (2024).
[127]F. Bouchet, "Is the Boltzmann equation reversible? A large deviation perspective on the irreversibility paradox," J. Stat. Phys. **181**, 515–550 (2020).
[128]T. Bodineau, I. Gallagher, L. Saint-Raymond, and S. Sergio, "Statistical dynamics of a hard sphere gas: Fluctuating Boltzmann equation and large deviations," Ann. Math. **198**, 1047–1201 (2023).
[129]J. J. Brey, P. Maynar, and M. I. García de Soria, "Fluctuating hydrodynamics for dilute granular gases," Phys. Rev. E **79**, 051305 (2009).
[130]P. Maynar, M. I. G. de Soria, and E. Trizac, "Fluctuating hydrodynamics for driven granular gases," Eur. Phys. J.: Spec. Top. **179**, 123–139 (2009).
[131]C. Scheibner, A. Souslov, D. Banerjee, P. Surówka, W. T. M. Irvine, and V. Vitelli, "Odd elasticity," Nat. Phys. **16**, 475–480 (2020).
[132]T. R. Kirkpatrick, S. P. Das, M. H. Ernst, and J. Piasecki, "Kinetic theory of transport in a hard sphere crystal," J. Chem. Phys. **92**, 3768–3780 (1990).
[133]B. Cleuren and C. Van den Broeck, "Granular Brownian motor," Europhys. Lett. **77**, 50003 (2007).
[134]G. Costantini, U. Marini Bettolo Marconi, and A. Puglisi, "Granular Brownian ratchet model," Phys. Rev. E **75**, 061124 (2007).
[135]C. Hargus, F. Ghimenti, J. Tailleur, and F. van Wijland, "Odd dynamics of passive objects in a chiral active bath," Phys. Rev. Lett. **135**, 167102 (2025).
[136]C. Hargus, F. Ghimenti, J. Tailleur, and F. van Wijland, "Passive objects in a chiral active bath: From microscopic to macroscopic," Phys. Rev. E **112**, 044127 (2025).
[137]A. R. Poggioli and D. T. Limmer, "Odd mobility of a passive tracer in a chiral active fluid," Phys. Rev. Lett. **130**, 158201 (2023).
[138]M. Chatzittofi and Y. Hosaka, "Dumbbell dimer dynamics in three-dimensional chiral fluids," Phys. Rev. E **112**, 055416 (2025).
[139]J. H. Irving and J. G. Kirkwood, "The statistical mechanical theory of transport processes. IV. The equations of hydrodynamics," J. Chem. Phys. **18**, 817–829 (1950).
[140]J. W. Dufty and J. J. Brey, "Green–Kubo expressions for a granular gas," J. Stat. Phys. **109**, 433–448 (2002).
[141]A. W. Lees and S. F. Edwards, "The computer study of transport processes under extreme conditions," J. Phys. C: Solid State Phys. **5**, 1921 (1972).
[142]J. Mabillard and P. Gaspard, "Hydrodynamic properties of the perfect hard-sphere crystal: Microscopic computations with Helfand moments," J. Stat. Mech.: Theory Exp. **2024**, 023208.
[143]S. Saha and M. Alam, "Normal stress differences, their origin and constitutive relations for a sheared granular fluid," J. Fluid Mech. **795**, 549–580 (2016).
[144]F. Müller-Plathe, "A simple nonequilibrium molecular dynamics method for calculating the thermal conductivity," J. Chem. Phys. **106**, 6082–6085 (1997).
[145]E. Helfand, "Transport coefficients from dissipation in a canonical ensemble," Phys. Rev. **119**, 1 (1960).
[146]C. Hargus, A. Deshpande, A. K. Omar, and K. K. Mandadapu, "Flux hypothesis for odd transport phenomena," Phys. Rev. Lett. **134**, 097105 (2025).
[147]J. W. Dufty, "Shear stress correlations in hard and soft sphere fluids," Mol. Phys. **100**, 2331–2336 (2002).
[148]J. J. Brey and M. J. Ruiz-Montero, "Simulation study of the Green–Kubo relations for dilute granular gases," Phys. Rev. E **70**, 051301 (2004).

15 July 2026 13:12:18

Published under an exclusive license by AIP Publishing